

# Fermionic parton theory of Rydberg $\mathbb{Z}_2$ quantum spin liquids

Atanu Maity,<sup>1,2</sup> Yasir Iqbal,<sup>2</sup> and Rhine Samajdar<sup>3,4,\*</sup>

<sup>1</sup>*Institut für Theoretische Physik und Astrophysik and Würzburg-Dresden Cluster of Excellence ct.qmat, Julius-Maximilians-Universität Würzburg, Am Hubland, Campus Süd, Würzburg 97074, Germany*

<sup>2</sup>*Department of Physics and Quantum Centre for Diamond and Emergent Materials (QuCenDiEM), Indian Institute of Technology Madras, Chennai 600036, India*

<sup>3</sup>*Department of Physics, Princeton University, Princeton, NJ 08544, USA*

<sup>4</sup>*Princeton Center for Theoretical Science, Princeton University, Princeton, NJ 08544, USA*

Programmable quantum simulators based on neutral atom arrays today offer powerful platforms for studying strongly correlated phases of quantum matter. Here, we employ the projective symmetry group framework to describe the symmetry fractionalization patterns in a topologically ordered  $\mathbb{Z}_2$  quantum spin liquid (QSL) synthesized in such a Rydberg array on the ruby lattice. By systematically comparing the static structure factors of *all* possible mean-field *Ansätze* against density-matrix renormalization group calculations, we identify a promising candidate for the precise  $\mathbb{Z}_2$  QSL realized microscopically. We also present detailed analyses of the dynamical structure factors as a reference for future experiments and showcase how these spin correlations can differentiate between varied QSL *Ansätze*.

*Introduction.*—Quantum spin liquids (QSLs) are fascinating strongly correlated phases of matter characterized by long-range many-body quantum entanglement [1]. The highly entangled nature of these quantum states lies at the root of their many exotic properties, such as emergent gauge fields [2, 3], and topological order beyond the Landau-Ginzburg paradigm of symmetry breaking [4]. Another such defining feature of QSLs is the presence of *fractionalized* excitations carrying quantum numbers that are fractions of those borne by the original degrees of freedom of the system.

Among the plethora of theoretically proposed QSL states, the simplest perhaps is the  $\mathbb{Z}_2$  spin liquid [5–7]. The  $\mathbb{Z}_2$  QSL is a gapped phase of matter which preserves all space-group and time-reversal symmetries and possesses the same topological order as the celebrated toric code [8]. In recent years, much effort has been devoted towards the search for such a  $\mathbb{Z}_2$  QSL in geometrically frustrated solid-state materials [9]. However, another particularly promising (and relatively new) direction is the realization of these QSL states in “synthetic” many-body systems.

Strongly interacting arrays of neutral atoms offer one such versatile platform for quantum simulation of spin models [10], using ensembles of optically pumped atoms interacting via excitations to high-lying Rydberg states. In these systems, a key constraint is imposed by the “Rydberg blockade” [11], which energetically forbids the simultaneous excitation of neighboring atoms and leads to a rich variety of physics in both one [12–16] and two [17–21] dimensions. In particular, under certain conditions, blockade-allowed configurations of Rydberg atoms can be mapped [22, 23] to close-packed states of so-called quantum dimer models [24, 25]. Based on this mapping,

recent beautiful experiments by Semeghini *et al.* [26] have demonstrated the synthesis of a topologically ordered  $\mathbb{Z}_2$  QSL—corresponding to a resonating valence bond state of dimers—in arrays of Rydberg atoms on the ruby lattice [27].

Importantly, just the  $\mathbb{Z}_2$  nature of the QSL alone does *not* fully specify the microscopic state; there can be many different types of  $\mathbb{Z}_2$  QSLs for the same lattice. This can be understood as a direct consequence of fractionalization: the correct degrees of freedom to describe the QSL are not the microscopic spin variables but rather the emergent fractionalized ones, termed “partons”. In the parton Hilbert space, however, any physical symmetry operation can also generically be accompanied by a gauge transformation. Stated otherwise, the symmetries act *projectively* in this space, and this projective action of lattice and time-reversal symmetries define and distinguish between various QSL states. For instance, Wen [28] famously showed that there are 272 distinct symmetric  $\mathbb{Z}_2$  QSL states for spin-rotation-invariant square-lattice systems. Therefore, the natural question to ask is, what are the possible  $\mathbb{Z}_2$  QSL states for the Rydberg array, and of these, which is the one realized microscopically?

In this Letter, we address this question using a two-pronged approach. The standard theoretical framework for constructing QSL states is parton mean-field theory [29–31]; adopting this approach, we describe our system in terms of emergent fermionic partons. Through a careful analysis of the projective symmetry group (PSG) [28, 32], we systematically classify all allowed  $\mathbb{Z}_2$  QSL states based on the symmetries of the ruby-lattice Rydberg system. A significant technical challenge in this regard (which has also previously complicated studies in strongly spin-orbit-coupled systems [33, 34]) is that the Rydberg Hamiltonian (see Eq. (1) below) does not possess an  $SU(2)$  spin-rotation symmetry; this introduces a large number of singlet and triplet terms to consider.

\* rhine\_samajdar@princeton.edu

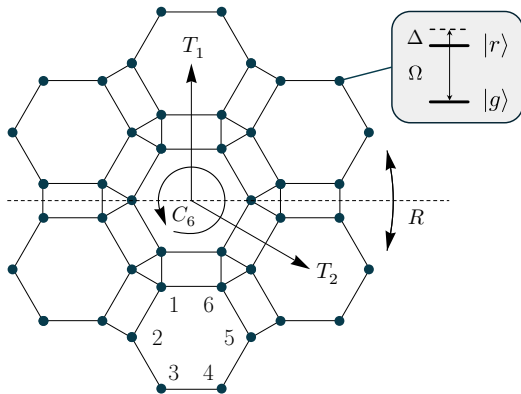


Figure 1. An illustration of the ruby lattice, highlighting the six sites in the unit cell and the space-group symmetry elements  $\{T_1, T_2, C_6, R\}$ . The spin at each site corresponds to a two-level system formed by the atomic ground and Rydberg states, with transitions between them driven by a laser with Rabi frequency  $\Omega$  and detuning  $\Delta$ .

Here, overcoming this difficulty, we build upon the classification scheme introduced for the spin-rotation-invariant case [35] and investigate the effects of breaking the global  $SU(2)$  symmetry.

Based on PSG considerations, we find a total of 50 realizable  $\mathbb{Z}_2$  QSLs. Then, we perform a systematic search in the parameter space of spinon mean-field Hamiltonians to identify from among these the most likely candidate for the Rydberg QSL state. We further characterize the spin correlations for these states, presenting in-depth predictions for static and dynamical structure factors, which can be measured in future experiments. Our analyses not only yield valuable insights into the microscopic nature of the Rydberg  $\mathbb{Z}_2$  QSL state but are also universal in that they rely solely on symmetries rather than the precise tuning parameters of the Hamiltonian.

*Model and parton construction.*—We consider an array of  $N$  Rydberg atoms positioned on the sites  $\{\mathbf{r}_i\}$  of the ruby lattice (Fig. 1). Each atom can be regarded as a two-level spin-1/2 system where the atomic ground ( $|g\rangle$ ) and Rydberg ( $|r\rangle$ ) states correspond to spin down and up, respectively. Defining  $S_i^x \equiv (|g\rangle_i \langle r| + \text{h.c.})/2$ ,  $n_i \equiv |r\rangle_i \langle r|$ , and  $S_i^z \equiv n_i - 1/2$ , the many-body Hamiltonian can be written as a long-ranged transverse-field Ising model in a longitudinal field [36, 37]:

$$H = \Omega \sum_i S_i^x - \Delta \sum_i n_i + \sum_{\langle i,j \rangle} V_{ij} n_i n_j. \quad (1)$$

Here,  $\Omega$  is the Rabi frequency of the laser that drives transitions between the ground and Rydberg states,  $\Delta$  is the laser detuning, and  $V_{ij} = V_0/|\mathbf{r}_i - \mathbf{r}_j|^6$  is a long-ranged van der Waals potential arising from the strong dipole-dipole interactions [10, 38].

On choosing the interatomic spacing such that up to third-nearest-neighboring atoms are mutually blocked, the Rydberg Hamiltonian on the ruby lattice is known

to host a  $\mathbb{Z}_2$  quantum spin liquid ground state [26]. This  $\mathbb{Z}_2$  QSL corresponds to the deconfined phase of a gauge theory [39, 40] and supports three species of quasiparticle excitations [41]: a bosonic “spinon” (called the  $e$  particle in the language of the toric code), a bosonic “vison” ( $m$ ) [42], and a fermionic spinon ( $\varepsilon = e \times m$ ). The time-honored method which facilitates the study of such fractionalized excitations and other emergent properties of the QSL state is the parton construction.

In the parton framework, the physical spins are decomposed into more fundamental degrees of freedom, which carry spin but no charge, thus allowing for a natural description of the fractionalization of quantum numbers. Mathematically, the spin operators on each lattice site are expressed in terms of two flavors of complex spin-1/2 fermionic quasiparticles (known as Abrikosov fermions). Denoting the two types of partons using a pseudospin index  $\sigma = \uparrow, \downarrow$ , we can write  $S_i^\gamma = (f_{i\sigma}^\dagger \tau_{\sigma\sigma'}^\gamma f_{i\sigma'})/2$ , where  $\tau^\gamma$  ( $\gamma = x, y, z$ ) is a Pauli matrix, and summation is implied over repeated indices. Such a rewriting enlarges the local Hilbert space, so, to remain in the physical subspace, we impose an additional constraint  $f_{i\sigma}^\dagger f_{i\sigma} = 1$ ,  $f_{i\sigma} f_{i\sigma'} \epsilon_{\sigma\sigma'} = 0$  [30, 31], ensuring that there is exactly one fermion on each site. Conveniently, the spin operator can now be recast using a spinor doublet  $\psi_i = (\phi_i, \bar{\phi}_i)$ , where  $\phi_i = (f_{i,\uparrow}, f_{i,\downarrow})^T$  and  $\bar{\phi}_i = (f_{i,\downarrow}^\dagger, -f_{i,\uparrow}^\dagger)^T$ , as  $S_i^\gamma = \text{Tr}[\psi_i^\dagger \tau^\gamma \psi_i]/2$  [43]; the associated half-filling constraint then reads  $\psi_i^\dagger \tau^\gamma \psi_i^\dagger = 0$ . A key consequence of this formulation is the emergence of a local gauge symmetry absent in the original spin Hamiltonian: the spin operators remain invariant under a site-dependent transformation  $\psi_i \rightarrow \psi_i W_i$ , for  $W_i \in SU(2)$ . As we show below, this emergent gauge symmetry bears important implications for the action of physical symmetry operations.

*Mean-field Ansatz.*—Next, we insert this fermionic representation of the spin operators into the Hamiltonian (1). Any two-spin interaction term (e.g.,  $n_i n_j$ ) in the original model, however, becomes a four-fermion term in the parton representation, so to make further analytical progress, we perform a quadratic mean-field decomposition [28]. There are two types of (matrix-valued) mean fields: singlets,  $u_{ij}^0 = \langle \psi_i^\dagger \psi_j \rangle$ , and (three) triplets,  $u_{ij}^\gamma = \langle \psi_i^\dagger \tau^\gamma \psi_j \rangle$ . In terms of these fields, any generic spin Hamiltonian can be written in the quadratic form [44] (see Supplemental Material (SM) [45] for details):

$$H_q = \sum_{\langle i,j \rangle} \text{Tr} \left[ \tau^\alpha \psi_i u_{ij}^\alpha \psi_j^\dagger + \text{h.c.} \right] + \sum_i \text{Tr} \left[ \tau^\alpha \psi_i u_{ii}^\alpha \psi_i^\dagger \right], \quad (2)$$

where  $\alpha = 0$  ( $\alpha = x, y, z$ ) corresponds to singlet (triplet) fields. The set of expectation values  $\{u_{ij}^\alpha\}$  define an *Ansatz* for QSL states. Each  $u_{ij}^\alpha$  can be parametrized using a basis of Pauli matrices as  $u_{ij}^0 = i s_{ij}^0 \tau^0 + s_{ij}^1 \tau^x + s_{ij}^2 \tau^y + s_{ij}^3 \tau^z$ , and  $u_{ij}^\gamma = t_{ij}^{\gamma,0} \tau^0 + i(t_{ij}^{\gamma,1} \tau^x + t_{ij}^{\gamma,2} \tau^y + t_{ij}^{\gamma,3} \tau^z)$ ,

No.	$\{\eta, \eta_{C_6}, \eta_R, \eta_{C_6R}, \eta_{\Theta C_6}\}$	$g_\Theta$	1NN		2NN		3NN		Onsite		IGG
			$\mathcal{U}_1^0$	$\mathcal{U}_1^z$	$\mathcal{U}_2^0$	$\mathcal{U}_2^z$	$\mathcal{U}_3^0$	$\mathcal{U}_3^z$	$\mathcal{U}_0^0$	$\mathcal{U}_0^z$	
1	$\{\eta, \pm\eta, +, +, +\}$	$i\tau^y$	$\tau^{x,z}$	$\tau^0$	$\tau^{x,z}$	$\tau^0$	$\tau^{x,z}/0$	$\tau^0/i\tau^y$	$\tau^{x,z}$	$\tau^0$	$\mathbb{Z}_2$
2	$\{\eta, \pm\eta, +, -, +\}$	$i\tau^y$	$\tau^{x,z}$	$\tau^0$	0	$i\tau^y$	$\tau^{x,z}/0$	$\tau^0/i\tau^y$	$\tau^{x,z}$	$\tau^0$	$\mathbb{Z}_2$
3	$\{\eta, \pm\eta, +, +, -\}$	$i\tau^y$	$\tau^{x,z}$	$\tau^0$	$\tau^y$	0	$\tau^y/i\tau^0$	$0/i\tau^{z,x}$	$\tau^{x,z}$	$\tau^0$	$\mathbb{Z}_2$
4	$\{\eta, \pm\eta, +, -, -\}$	$i\tau^y$	$\tau^{x,z}$	$\tau^0$	$i\tau^0$	$i\tau^{x,z}$	$\tau^y/i\tau^0$	$0/i\tau^{z,x}$	$\tau^{x,z}$	$\tau^0$	$\mathbb{Z}_2$
5	$\{\eta, \pm\eta, -, +, +\}$	$i\tau^y$	$\tau^z$	$\tau^0, i\tau^y$	$\tau^z$	$\tau^0, i\tau^y$	$\tau^{x,z}/0$	$\tau^0/i\tau^y$	$\tau^z$	$\tau^0$	$\mathbb{Z}_2$
6	$\{\eta, \pm\eta, -, -, +\}$	$i\tau^y$	$\tau^z$	$\tau^0, i\tau^y$	$\tau^x$	0	$\tau^{x,z}/0$	$\tau^0/i\tau^y$	$\tau^z$	$\tau^0$	$\mathbb{Z}_2$
7	$\{\eta, \pm\eta, -, +, -\}$	$i\tau^y$	$\tau^z$	$\tau^0, i\tau^y$	0	$i\tau^x$	$\tau^y/i\tau^0$	$0/i\tau^{x,z}$	$\tau^z$	$\tau^0$	$\mathbb{Z}_2$
8	$\{\eta, \pm\eta, -, -, -\}$	$i\tau^y$	$\tau^z$	$\tau^0, i\tau^y$	$i\tau^0, \tau^y$	$i\tau^z$	$\tau^y/i\tau^0$	$0/i\tau^{x,z}$	$\tau^z$	$\tau^0$	$\mathbb{Z}_2$
9	$\{\eta, \pm\eta, -, -, +\}$	$i\tau^z$	0	$\tau^0$	$\tau^{x,y}$	$i\tau^z$	$\tau^{x,y}/0$	$\tau^0/i\tau^z$	0	$\tau^0$	$\mathbb{Z}_2$
10	$\{\eta, \pm\eta, -, +, -\}$	$i\tau^z$	0	$\tau^0$	$\tau^z$	$i\tau^{x,y}$	$\tau^z/i\tau^0$	$0/i\tau^{x,y}$	0	$\tau^0$	$\mathbb{Z}_2$
11	$\{\eta, \pm\eta, -, +, -\}$	$\tau^0$	0	$\tau^0, i\tau^{x,y}$	$\tau^z$	0	$\tau^{x,y,z}/i\tau^0$	0	0	$\tau^0$	$\mathbb{Z}_2$
12	$\{\eta, \pm\eta, -, -, -\}$	$\tau^0$	0	$\tau^0, i\tau^{x,y}$	$i\tau^0, \tau^{x,y}$	0	$\tau^{x,y,z}/i\tau^0$	0	0	$\tau^0$	$\mathbb{Z}_2$
13	$\{\eta, \pm\eta, +, +, -\}$	$\tau^0$	0	$\tau^0$	$\tau^{x,y,z}$	0	$\tau^{x,y,z}/i\tau^0$	0	0	$\tau^0$	$\mathbb{Z}_2/\text{U}(1)$
14	$\{\eta, \pm\eta, +, -, -\}$	$\tau^0$	0	$\tau^0$	$i\tau^0$	0	$\tau^{x,y,z}/i\tau^0$	0	0	$\tau^0$	$\text{U}(1)$
15	$\{\eta, \pm\eta, -, +, +\}$	$i\tau^z$	0	$\tau^0$	0	$\tau^0$	$\tau^{x,y}/0$	$\tau^0/i\tau^z$	0	$\tau^0$	$\text{U}(1)$
16	$\{\eta, \pm\eta, -, -, -\}$	$i\tau^z$	0	$\tau^0$	$i\tau^0$	0	$\tau^z/i\tau^0$	$0/i\tau^{x,y}$	0	$\tau^0$	$\text{U}(1)$

Table I. All possible  $\{T_1, T_2, R, C_6, \Theta\} \times \text{U}(1)_{\text{spin}}$ -symmetric mean field *Ansätze* with up to third-nearest-neighbor hopping and pairing terms. In the chosen gauge, the onsite terms are uniform, i.e.,  $u_{ii}^\alpha = \mathcal{U}_0^\alpha$ . Each row gives rise to four *Ansätze* with different combinations of  $\eta = \pm 1$ ,  $\eta_{C_6} = \pm \eta$ . In the “3NN” and “IGG” columns above, the term on the left (right) side of “/” corresponds to  $\eta_{C_6} = +\eta$  ( $\eta_{C_6} = -\eta$ ).

for real coefficients  $s_{ij}$ ,  $t_{ij}$ . In this basis, satisfying the requirement that  $u_{ji}^\alpha = u_{ij}^{\alpha\dagger}$  restricts certain onsite terms as  $s_{ii}^0 = t_{ii}^{\gamma,1} = t_{ii}^{\gamma,2} = t_{ii}^{\gamma,3} = 0$ . Note that  $u_{ii}^0$  incorporates the constraint of having one fermion per site at a mean-field level, and  $s_{ii}^1$ ,  $s_{ii}^2$ ,  $s_{ii}^3$  are the associated Lagrange multipliers.

*PSG classification.*—So far, while we have written down the most generic possible quadratic parton Hamiltonian in Eq. (2), we are yet to specify the spatial structure of  $u_{ij}^\alpha$ . In order to do so, we need to consider the symmetries of the system, which will significantly constrain the terms allowed.

The space group of the ruby lattice is  $p6m$  and is generated by two lattice translations ( $T_1, T_2$ ), a sixfold rotation ( $C_6$ ) around an axis perpendicular to the plane, and a reflection ( $R$ ) about the  $x$ -axis (Fig. 1). On the Hamiltonian, these lattice symmetries act as  $S_i^\gamma \rightarrow S_{\mathcal{O}(i)}^\gamma$  with  $\mathcal{O} \in \{T_1, T_2, C_6, R\}$  [46]. Furthermore, one can identify an anti-unitary time-reversal symmetry  $\Theta$  under which  $S_i^\gamma \rightarrow (-)^{\delta_{\gamma,y}} S_i^\gamma$ ; this may be understood as the combination of “conventional” time reversal (which sends  $\mathbf{S}_i \rightarrow -\mathbf{S}_i$ ) and a global spin rotation by  $\pi$  about the  $S^y$ -axis.

Acting with the operator  $S_i^x$  on the Rydberg QSL creates two  $e$  particles [39], resulting in an excited state which is orthogonal to the ground state. Hence, we can approximate  $\langle S_i^x \rangle \approx 0$  (although  $\langle \prod_{i \in \ell} S_i^x \rangle$  along a closed loop  $\ell$  may be nonzero). Consequently, all terms in the Hamiltonian (2) which would contribute to a nonvanishing expectation value of  $S^x$  can be reasonably ne-

glected. These mean fields are precisely the transverse triplet components:  $u_{ij}^x$  and  $u_{ij}^y$ . This allows us to consider *Ansätze* consisting of only singlet ( $u_{ij}^0$ ) and longitudinal triplet ( $u_{ij}^z$ ) fields; the latter lead to  $\langle S_i^z \rangle \neq 0$ , as required for a nonzero Rydberg excitation density. Thus, while the lattice Hamiltonian does not possess an  $\text{SU}(2)$  spin-rotation symmetry, at the level of the fermionic mean-field wavefunction, the restriction of the triplet fields to only longitudinal components yields an emergent  $\text{U}(1)_{\text{spin}}$  symmetry.

Having established the symmetry group, our next step is to identify all possible *Ansätze* that are consistent with this set of symmetries. However, the definition of symmetry invariance in the parton Hilbert space is rather nontrivial due to the aforementioned  $\text{SU}(2)$  gauge freedom. To wit, under the transformation  $\psi_i \rightarrow \psi_i W_i$  and  $u_{ij}^\alpha \rightarrow W_i^\dagger u_{ij}^\alpha W_j$ , with  $W_i \in \text{SU}(2)$ ,  $H_q$  remains invariant, so two *Ansätze*  $u_{ij}^\alpha$  and  $\tilde{u}_{ij}^\alpha = W_i^\dagger u_{ij}^\alpha W_j$  represent the same physical state. This property defines the projective action of symmetry operations as follows. Consider an element of the symmetry group  $\mathcal{O}$  which acts on an *Ansatz* as  $\mathcal{O} : u_{ij}^\alpha \rightarrow \tilde{u}_{ij}^\alpha$ . Even if  $u_{ij}^\alpha \neq \tilde{u}_{ij}^\alpha$ , the symmetry under  $\mathcal{O}$  is preserved if  $\exists W_{\mathcal{O},i} \in \text{SU}(2)$  such that  $u_{ij}^\alpha = W_{\mathcal{O},i}^\dagger \tilde{u}_{ij}^\alpha W_{\mathcal{O},j}$ . The combined operation of  $\mathcal{O}$  and its accompanying  $\text{SU}(2)$  gauge transformation  $W_{\mathcal{O},i}$  defines the PSG. Therefore, the way to identify different *Ansätze* representing distinct QSLs states at the mean-field level is to find all possible gauge-inequivalent projective symmetry actions  $W_{\mathcal{O},i}$  for  $\mathcal{O} \in \{\mathbb{1}, T_1, T_2, C_6, R, \Theta\}$  ( $\mathbb{1}$  being the identity element). The projective action of

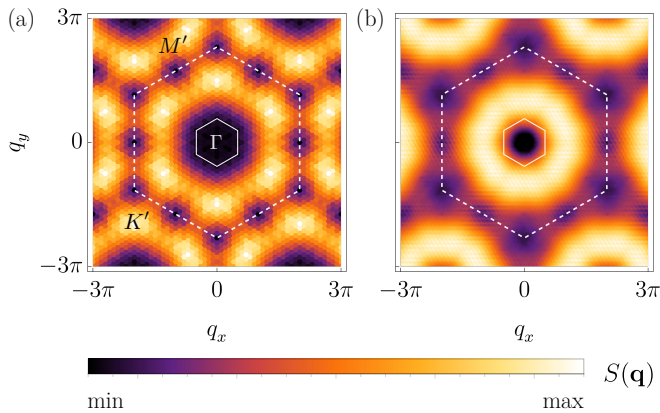


Figure 2. (a) Static structure factor of the Rydberg  $\mathbb{Z}_2$  QSL, as determined from the DMRG ground state on a 288-site lattice. (b) SSF for the *Ansatz* in row 8 of Table I with  $\eta = -\eta_{C_6} = 1$  for (optimized) mean-field amplitudes chosen to be  $|\mathcal{U}_2^\alpha|/|\mathcal{U}_1^\alpha| = r = 1.25$ ,  $t_{ij}^{z,\alpha} = 2s_{ij}^{0,\alpha}$ , and  $t_{ii}^{z,0} = 0.35$ . While there are quantitative differences between the two SSFs, the qualitative similarity in the locations of their minima and maxima is apparent. The dashed (solid) hexagons mark the extended (first) Brillouin zone.

the identity  $W_1$  defines a subgroup of the PSG known as the invariant gauge group (IGG), i.e., the group of operations that leave the *Ansatz* unchanged. The IGG determines the nature of low-energy fluctuations about the mean-field solutions, and—depending on the allowed mean-field parameters—is broken down here from  $SU(2)$  to either  $U(1)$  or  $\mathbb{Z}_2$ .

Expanding on a recent PSG classification [35] of spin-liquid states on the ruby lattice [47], here, we determine the possible symmetric mean-field *Ansätze* for the Rydberg QSL. Table I lists all such *Ansätze* for up to third-nearest-neighbor (3NN) couplings including, crucially, the triplet terms absent for the Heisenberg models considered in Ref. 35. Every *Ansatz* is labeled by a set of parameters  $\{\eta, \eta_{C_6}, \eta_R, \eta_{C_6R}, \eta_{\Theta C_6}\}$ , each of which can take values  $\pm 1$ , with  $\eta_{\Theta}$  originating from the gauge-enriched symmetry relations of the operation  $\mathcal{O}$  [45]. Additionally, one also has to specify a Pauli matrix associated with the action of time-reversal symmetry, which we denote by  $g_{\Theta}$  in Table I.

Although we begin with 64  $\mathbb{Z}_2$  projective extensions of the symmetry group, we find that only 50 of them can be realized with a  $\mathbb{Z}_2$  IGG—which is the case of interest given the  $\mathbb{Z}_2$  nature of the Rydberg QSL; the remaining correspond to a  $U(1)$  IGG. As Table I conveys, the whole *Ansatz* can be constructed from the knowledge of a few reference mean fields. Let us define the reference onsite, 1NN, 2NN, and 3NN fields as  $\mathcal{U}_0^\alpha$ ,  $\mathcal{U}_1^\alpha$ ,  $\mathcal{U}_2^\alpha$ , and  $\mathcal{U}_3^\alpha$ , respectively (see SM [45]); these can be read off from Table I. Then,  $u_{ij}^\alpha$  on all other bonds of the lattice can be obtained from these eight simply by symmetry, as detailed in the SM [45].

*Spin correlations of the Rydberg QSL.*—With the full

list of possible QSL states in hand, we now turn to examining the experimental signatures of the different  $\mathbb{Z}_2$  *Ansätze*. To this end, we compute the static structure factor (SSF)  $S(\mathbf{q})$ , which is the Fourier transform of the equal-time spin-spin correlation function; here, we specifically look at the  $z$ -component  $\langle S_i^z S_j^z \rangle$  since measurements in the computational basis are the most convenient experimentally.

To begin, we evaluate  $S(\mathbf{q})$  for the ground state of the Rydberg Hamiltonian in the QSL phase, as obtained on a 288-site lattice using the density-matrix renormalization group (DMRG) algorithm. The SSF, shown in Fig. 2(a), does not display any sharp Bragg peaks, as expected for a QSL, but does reveal two prominent features. First, the local minima of  $S(\mathbf{q})$  are located not only at the  $\Gamma$  (center) and  $K'$  (corner) points of the extended Brillouin zone, but also at the  $M'$  (edge) points. Secondly, the SSF exhibits a local maximum along the lines connecting the  $\Gamma$  and  $K'$  points.

These observations suggest a route towards identifying which *Ansatz* likely describes the microscopic QSL state realized for the Rydberg Hamiltonian. To do so, we focus on mean-field parameters which are set to a uniform value on all the 1NN bonds, and likewise for the 2NN bonds, but with the ratio between the two chosen to be  $1 : r$ . Systematically tuning  $r$ , we then compute  $S(\mathbf{q})$  for each *Ansatz* and inspect it for the properties identified above. Examining the nearly 300 SSFs in the SM, we find one promising QSL state (labeled  $8\{+, -, -, -, -\}$  in the notation of Table I) that is consistent with those features in a certain parameter regime. Optimizing further over the ratio of the singlet to triplet strengths for this candidate state, we see that it indeed shows good agreement with the characteristic features of the numerically computed SSF, as presented in Fig. 2(b).

Finally, we also study the dynamical structure factor (DSF):  $\mathcal{S}(\mathbf{q}, \omega) \equiv \int_{-\infty}^{+\infty} dt / (2\pi N^2) e^{i\omega t} \sum_{i,j} e^{i\mathbf{q} \cdot (\mathbf{r}_i - \mathbf{r}_j)} \times [\langle S_i^z(t) S_j^z(0) \rangle - \langle S_i^z(t) \rangle \langle S_j^z(0) \rangle]$ . The  $\omega$ -integrated version of this quantity is simply the SSF, but  $\mathcal{S}(\mathbf{q}, \omega)$  allows

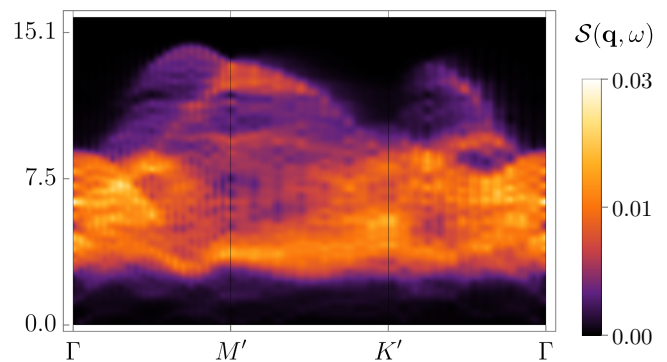


Figure 3. Dynamical structure factor, plotted along a high-symmetry path in the extended Brillouin zone, for the *Ansatz*  $8\{+, -, -, -, -\}$  with the same parameters as in Fig. 2(b).

us to probe  $\omega$ -resolved information about the excitation spectrum characterizing the low-energy response of the QSL state. Figure 3 illustrates the DSF for the candidate  $8\{+, -, -, -, -\}$  state (the DSFs of all other  $\mathbb{Z}_2$  *Ansätze* are tabulated in the SM for various values of  $r$  [45]). Clearly, we see that the state is gapped and that the scattering is diffuse with no sharp dispersive features. The fact that the DSF exhibits such a broad continuum can be interpreted as a distinctive signature of fractionalization [48].

*Discussion and outlook.*—Motivated by the observation of a  $\mathbb{Z}_2$  QSL in recent experiments on Rydberg atom arrays, in this work, we present a detailed projective symmetry group analysis of all possible mean-field *Ansätze* on the ruby lattice that could describe this state. We characterize these *Ansätze* by computing their associated static and dynamical structure factors and show how the low-energy spin correlations can distinguish between different QSL states. Our work should thus serve as a guide to future experiments, in which one could, say, measure the DSF [49] and compare it against our comprehensive listing in the SM [45] to identify the microscopic QSL state. In fact, here, we identify a promising candidate state using a similar procedure but based on numerical (DMRG) rather than experimental input. For comparison, it would also be interesting to theoretically calculate the structure factors of the Rydberg QSL using large-scale quantum Monte Carlo simulations [50, 51] of kagome-lattice dimer models [52].

Of course, strictly speaking, the mean-field wavefunction obtained from any *Ansatz* should be projected into the single-fermion-per-site subspace through numerical Gutzwiller projection methods [29] to obtain the true wavefunction in the original spin Hilbert space. While the Gutzwiller projection does affect the energetics, one does not expect the gauge fluctuations (which are gapped and thus mediate only short-range interactions) to qualitatively alter the properties of our mean-field state. We defer a complete analysis of the effects of such Gutzwiller projection to future work.

While we have focused here on a fermionic parton construction, the Rydberg  $\mathbb{Z}_2$  QSL state can also be described by a bosonic theory in which fractionalized bosonic quasiparticles live on the kagome [53] or the dice [54, 55] lattice; understanding the PSG classification of the latter is an important open question. Finally, our work also directly paves the way to developing variational descriptions of other species of Rydberg spin liquids—for instance, with either different emergent gauge groups [56–58] or spin chirality [59]—as well as higher-spin models [60, 61].

*Acknowledgments.*—We thank Subir Sachdev, Yanting Teng, and Ronny Thomale for useful discussions. This work was initiated and completed at the Aspen Center for Physics, which is supported by National Science Foundation grant PHY-2210452 and a

grant from the Simons Foundation (1161654, Troyer). This research was also supported in part by grant NSF PHY-2309135 to the Kavli Institute for Theoretical Physics (KITP) during the “A New Spin on Quantum Magnets” program in summer 2023. A. M. was supported by DFG Grant No. 258499086-SFB 1170 and the Würzburg-Dresden Cluster of Excellence on Complexity and Topology in Quantum Matter, Grant No. 390858490-EXC 2147. Y. I. acknowledges support from the ICTP through the Associates Programme, from the Simons Foundation through Grant No. 284558FY19, and from IIT Madras through the Institute of Eminence (IoE) program for establishing QuCenDiEM (Project No. SP22231244CPETWOCQDHOC). Y. I. also acknowledges the use of the computing resources at HPCE, IIT Madras. R. S. is supported by the Princeton Quantum Initiative Fellowship.

- 
- [1] L. Savary and L. Balents, Quantum spin liquids: a review, *Rep. Prog. Phys.* **80**, 016502 (2016).
  - [2] J. Knolle and R. Moessner, A field guide to spin liquids, *Annu. Rev. Condens. Matter Phys.* **10**, 451 (2019).
  - [3] C. Broholm, R. J. Cava, S. A. Kivelson, D. G. Nocera, M. R. Norman, and T. Senthil, Quantum spin liquids, *Science* **367**, eaay0668 (2020).
  - [4] X.-G. Wen, Colloquium: Zoo of quantum-topological phases of matter, *Rev. Mod. Phys.* **89**, 041004 (2017).
  - [5] N. Read and S. Sachdev, Large-N expansion for frustrated quantum antiferromagnets, *Phys. Rev. Lett.* **66**, 1773 (1991).
  - [6] X. G. Wen, Mean-field theory of spin-liquid states with finite energy gap and topological orders, *Phys. Rev. B* **44**, 2664 (1991).
  - [7] S. Sachdev, Kagomé- and triangular-lattice Heisenberg antiferromagnets: Ordering from quantum fluctuations and quantum-disordered ground states with unconfined bosonic spinons, *Phys. Rev. B* **45**, 12377 (1992).
  - [8] A. Kitaev, Anyons in an exactly solved model and beyond, *Ann. Phys.* **321**, 2 (2006).
  - [9] P. A. Lee, An end to the drought of quantum spin liquids, *Science* **321**, 1306 (2008).
  - [10] H. Bernien, S. Schwartz, A. Keesling, H. Levine, A. Omran, H. Pichler, S. Choi, A. S. Zibrov, M. Endres, M. Greiner, V. Vuletić, and M. D. Lukin, Probing many-body dynamics on a 51-atom quantum simulator, *Nature* **551**, 579 (2017).
  - [11] D. Jaksch, J. I. Cirac, P. Zoller, S. L. Rolston, R. Côté, and M. D. Lukin, Fast quantum gates for neutral atoms, *Phys. Rev. Lett.* **85**, 2208 (2000).
  - [12] A. Keesling, A. Omran, H. Levine, H. Bernien, H. Pichler, S. Choi, R. Samajdar, S. Schwartz, P. Silvi, S. Sachdev, P. Zoller, M. Endres, M. Greiner, V. Vuletić, and M. D. Lukin, Quantum Kibble-Zurek mechanism and critical dynamics on a programmable Rydberg simulator, *Nature* **568**, 207 (2019).
  - [13] R. Samajdar, S. Choi, H. Pichler, M. D. Lukin, and S. Sachdev, Numerical study of the chiral  $\mathbb{Z}_3$  quantum phase transition in one spatial dimension, *Phys. Rev. A*

- 98**, 023614 (2018).
- [14] S. Whitsitt, R. Samajdar, and S. Sachdev, Quantum field theory for the chiral clock transition in one spatial dimension, *Phys. Rev. B* **98**, 205118 (2018).
- [15] N. Chepiga and F. Mila, Floating Phase versus Chiral Transition in a 1D Hard-Boson Model, *Phys. Rev. Lett.* **122**, 017205 (2019).
- [16] S. de Léséleuc, V. Lienhard, P. Scholl, D. Barredo, S. Weber, N. Lang, H. P. Büchler, T. Lahaye, and A. Browaeys, Observation of a symmetry-protected topological phase of interacting bosons with Rydberg atoms, *Science* **365**, 775 (2019).
- [17] R. Samajdar, W. W. Ho, H. Pichler, M. D. Lukin, and S. Sachdev, Complex Density Wave Orders and Quantum Phase Transitions in a Model of Square-Lattice Rydberg Atom Arrays, *Phys. Rev. Lett.* **124**, 103601 (2020).
- [18] S. Ebadi, T. T. Wang, H. Levine, A. Keesling, G. Semeghini, A. Omran, D. Bluvstein, R. Samajdar, H. Pichler, W. W. Ho, S. Choi, S. Sachdev, M. Greiner, V. Vuletić, and M. D. Lukin, Quantum phases of matter on a 256-atom programmable quantum simulator, *Nature* **595**, 227 (2021).
- [19] P. Scholl, M. Schuler, H. J. Williams, A. A. Eberharter, D. Barredo, K.-N. Schymik, V. Lienhard, L.-P. Henry, T. C. Lang, T. Lahaye, A. M. Läuchli, and A. Browaeys, Quantum simulation of 2D antiferromagnets with hundreds of Rydberg atoms, *Nature* **595**, 233 (2021).
- [20] M. Kalinowski, R. Samajdar, R. G. Melko, M. D. Lukin, S. Sachdev, and S. Choi, Bulk and boundary quantum phase transitions in a square Rydberg atom array, *Phys. Rev. B* **105**, 174417 (2022).
- [21] C. Chen, G. Bornet, M. Bintz, G. Emperauger, L. Leclerc, V. S. Liu, P. Scholl, D. Barredo, J. Hauschild, S. Chatterjee, M. Schuler, A. M. Läuchli, M. P. Zaletel, T. Lahaye, N. Y. Yao, and A. Browaeys, Continuous symmetry breaking in a two-dimensional Rydberg array, *Nature* **616**, 691–695 (2023).
- [22] R. Samajdar, W. W. Ho, H. Pichler, M. D. Lukin, and S. Sachdev, Quantum phases of Rydberg atoms on a kagome lattice, *Proc. Natl. Acad. Sci. U.S.A.* **118**, e2015785118 (2021), 2011.12295.
- [23] R. Verresen, M. D. Lukin, and A. Vishwanath, Prediction of Toric Code Topological Order from Rydberg Blockade, *Phys. Rev. X* **11**, 031005 (2021).
- [24] D. S. Rokhsar and S. A. Kivelson, Superconductivity and the Quantum Hard-Core Dimer Gas, *Phys. Rev. Lett.* **61**, 2376 (1988).
- [25] R. Moessner and K. S. Raman, Quantum dimer models, in *Introduction to Frustrated Magnetism* (Springer, 2011) pp. 437–479.
- [26] G. Semeghini, H. Levine, A. Keesling, S. Ebadi, T. T. Wang, D. Bluvstein, R. Verresen, H. Pichler, M. Kalinowski, R. Samajdar, A. Omran, S. Sachdev, A. Vishwanath, M. Greiner, V. Vuletić, and M. D. Lukin, Probing topological spin liquids on a programmable quantum simulator, *Science* **374**, 1242 (2021).
- [27] G. Giudici, M. D. Lukin, and H. Pichler, Dynamical preparation of quantum spin liquids in Rydberg atom arrays, *Phys. Rev. Lett.* **129**, 090401 (2022).
- [28] X.-G. Wen, Quantum orders and symmetric spin liquids, *Phys. Rev. B* **65**, 165113 (2002).
- [29] X.-G. Wen, *Quantum Field Theory of Many-Body Systems* (Oxford University Press, 2007).
- [30] G. Baskaran, Z. Zou, and P. Anderson, The resonating valence bond state and high- $T_c$  superconductivity — A mean field theory, *Solid State Commun.* **63**, 973 (1987).
- [31] G. Baskaran and P. W. Anderson, Gauge theory of high-temperature superconductors and strongly correlated Fermi systems, *Phys. Rev. B* **37**, 580 (1988).
- [32] X.-G. Wen, Quantum order: a quantum entanglement of many particles, *Phys. Lett. A* **300**, 175 (2002).
- [33] T. Dodds, S. Bhattacharjee, and Y. B. Kim, Quantum spin liquids in the absence of spin-rotation symmetry: Application to herbertsmithite, *Phys. Rev. B* **88**, 224413 (2013).
- [34] J. Reuther, S.-P. Lee, and J. Alicea, Classification of spin liquids on the square lattice with strong spin-orbit coupling, *Phys. Rev. B* **90**, 174417 (2014).
- [35] A. Maity, R. Samajdar, and Y. Iqbal, Gapped and gapless quantum spin liquids on the ruby lattice (2024).
- [36] S. Sachdev, K. Sengupta, and S. M. Girvin, Mott insulators in strong electric fields, *Phys. Rev. B* **66**, 075128 (2002).
- [37] P. Fendley, K. Sengupta, and S. Sachdev, Competing density-wave orders in a one-dimensional hard-boson model, *Phys. Rev. B* **69**, 075106 (2004).
- [38] M. D. Lukin, M. Fleischhauer, R. Cote, L. M. Duan, D. Jaksch, J. I. Cirac, and P. Zoller, Dipole Blockade and Quantum Information Processing in Mesoscopic Atomic Ensembles, *Phys. Rev. Lett.* **87**, 037901 (2001).
- [39] R. Samajdar, D. G. Joshi, Y. Teng, and S. Sachdev, Emergent  $\mathbb{Z}_2$  gauge theories and topological excitations in Rydberg atom arrays, *Phys. Rev. Lett.* **130**, 043601 (2023).
- [40] P. S. Tarabunga, F. M. Surace, R. Andreoni, A. Angelone, and M. Dalmonte, Gauge-Theoretic Origin of Rydberg Quantum Spin Liquids, *Phys. Rev. Lett.* **129**, 195301 (2022).
- [41] N. Read and B. Chakraborty, Statistics of the excitations of the resonating-valence-bond state, *Phys. Rev. B* **40**, 7133 (1989).
- [42] T. Senthil and M. P. A. Fisher,  $\mathbb{Z}_2$  gauge theory of electron fractionalization in strongly correlated systems, *Phys. Rev. B* **62**, 7850 (2000).
- [43] I. Affleck, Z. Zou, T. Hsu, and P. W. Anderson, SU(2) gauge symmetry of the large- $U$  limit of the Hubbard model, *Phys. Rev. B* **38**, 745 (1988).
- [44] C. Liu, G. B. Halász, and L. Balents, Symmetric U(1) and  $\mathbb{Z}_2$  spin liquids on the pyrochlore lattice, *Phys. Rev. B* **104**, 054401 (2021).
- [45] See Supplemental Material for details on the PSG classification, the mean-field decoupling of the Rydberg Hamiltonian, and analyses of static and dynamical spin structure factors.
- [46] Since the “spin” here simply represents a binary degree of freedom encoded in two atomic levels, it does not transform as a pseudovector.
- [47] The definition of time reversal in Ref. 35 as  $\mathcal{T} : \hat{S}_i^\gamma \rightarrow -\hat{S}_i^\gamma$  differs from  $\Theta$ , but since the lattice coordinates do not change under either  $\mathcal{T}$  or  $\Theta$  and all other symmetry operators commute with both of them, we can use the same PSG classification.
- [48] R. Coldea, D. A. Tennant, and Z. Tylczynski, Extended scattering continua characteristic of spin fractionalization in the two-dimensional frustrated quantum magnet  $\text{Cs}_2\text{CuCl}_4$  observed by neutron scattering, *Phys. Rev. B* **68**, 134424 (2003).
- [49] P. Uhrich, S. Castrignano, H. Uys, and M. Kastner, Non-

- invasive measurement of dynamic correlation functions, *Phys. Rev. A* **96**, 022127 (2017).
- [50] Z. Yan, R. Samajdar, Y.-C. Wang, S. Sachdev, and Z. Y. Meng, Triangular lattice quantum dimer model with variable dimer density, *Nat. Commun.* **13**, 5799 (2022).
- [51] Z. Wang and L. Pollet, The renormalized classical spin liquid on the ruby lattice (2024), [arXiv:2406.07110 \[cond-mat.str-el\]](#).
- [52] G. Misguich, D. Serban, and V. Pasquier, Quantum Dimer Model on the Kagome Lattice: Solvable Dimer-Liquid and Ising Gauge Theory, *Phys. Rev. Lett.* **89**, 137202 (2002).
- [53] F. Wang and A. Vishwanath, Spin-liquid states on the triangular and Kagomé lattices: A projective-symmetry-group analysis of Schwinger boson states, *Phys. Rev. B* **74**, 174423 (2006).
- [54] Y. Huh, M. Punk, and S. Sachdev, Vison states and confinement transitions of  $\mathbb{Z}_2$  spin liquids on the kagome lattice, *Phys. Rev. B* **84**, 094419 (2011).
- [55] Y. Teng *et al.*, Vison excitations in Rydberg atom arrays (2024), in preparation.
- [56] G. Giudice, F. M. Surace, H. Pichler, and G. Giudici, Trimer states with  $\mathbb{Z}_3$  topological order in Rydberg atom arrays, *Phys. Rev. B* **106**, 195155 (2022).
- [57] M. Kornjača, R. Samajdar, T. Macrì, N. Gemelke, S.-T. Wang, and F. Liu, Trimer quantum spin liquid in a honeycomb array of Rydberg atoms, *Commun. Phys.* **6**, 358 (2023).
- [58] M. Bintz, V. S. Liu, J. Hauschild, A. Khalifa, S. Chatterjee, M. P. Zaletel, and N. Y. Yao, Dirac spin liquid in quantum dipole arrays (2024), [arXiv:2406.00098 \[cond-mat.str-el\]](#).
- [59] P. S. Tarabunga, G. Giudici, T. Chanda, and M. Dalmonde, Classification and emergence of quantum spin liquids in chiral Rydberg models, *Phys. Rev. B* **108**, 075118 (2023).
- [60] L. Homeier, T. J. Harris, T. Blatz, S. Geier, S. Hollerith, U. Schollwöck, F. Grusdt, and A. Bohrdt, Antiferromagnetic Bosonic  $t$ - $J$  Models and Their Quantum Simulation in Tweezer Arrays, *Phys. Rev. Lett.* **132**, 230401 (2024).
- [61] V. S. Liu, M. Bintz, M. Block, R. Samajdar, J. Kemp, and N. Y. Yao, Supersolidity and Simplex Phases in Spin-1 Rydberg Atom Arrays (2024), [arXiv:2407.17554 \[cond-mat.quant-gas\]](#).

# Supplemental Material for “Fermionic parton theory of Rydberg $\mathbb{Z}_2$ quantum spin liquids”

Atanu Maity,<sup>1,2</sup> Yasir Iqbal,<sup>2</sup> and Rhine Samajdar<sup>3,4</sup>

<sup>1</sup>*Institut für Theoretische Physik und Astrophysik and Würzburg-Dresden Cluster of Excellence ct.qmat, Julius-Maximilians-Universität Würzburg, Am Hubland, Campus Süd, Würzburg 97074, Germany*

<sup>2</sup>*Department of Physics and Quantum Centre for Diamond and Emergent Materials (QuCenDiEM), Indian Institute of Technology Madras, Chennai 600036, India*

<sup>3</sup>*Department of Physics, Princeton University, Princeton, NJ 08544, USA*

<sup>4</sup>*Princeton Center for Theoretical Science, Princeton University, Princeton, NJ 08544, USA*

In this Supplemental Material, we provide further details on the projective symmetry group (PSG) classification on the ruby lattice and the mean-field decoupling of the Rydberg Hamiltonian in the fermionic parton language. We also analytically compute and showcase the static as well as dynamical spin structure factors for all the identified *Ansätze* over a broad range of mean-field parameters.

## SI. SYMMETRIES AND PSG CLASSIFICATION

On the ruby lattice, the Rydberg Hamiltonian defined in Eq. (1) of the main text is explicitly invariant under the following symmetry transformations:

$$T_1 : (S_i^x, S_i^y, S_i^z) \rightarrow (S_{T_1(i)}^x, S_{T_1(i)}^y, S_{T_1(i)}^z), \quad (\text{S1})$$

$$T_2 : (S_i^x, S_i^y, S_i^z) \rightarrow (S_{T_2(i)}^x, S_{T_2(i)}^y, S_{T_2(i)}^z), \quad (\text{S2})$$

$$C_6 : (S_i^x, S_i^y, S_i^z) \rightarrow (S_{C_6(i)}^x, S_{C_6(i)}^y, S_{C_6(i)}^z), \quad (\text{S3})$$

$$R : (S_i^x, S_i^y, S_i^z) \rightarrow (S_{R(i)}^x, S_{R(i)}^y, S_{R(i)}^z), \quad (\text{S4})$$

$$\Theta : (S_i^x, S_i^y, S_i^z) \rightarrow (S_i^x, -S_i^y, S_i^z). \quad (\text{S5})$$

Here,  $T_1(i)$  and  $T_2(i)$  denote translations of the lattice coordinate  $i$  by the lattice vectors  $\mathbf{T}_1$  and  $\mathbf{T}_2$ , respectively,  $C_6(i)$  implements a sixfold rotation around the axis perpendicular to the plane, and  $R(i)$  represents a reflection about the  $x$ -axis. Note that time reversal  $\Theta$  does not act on the lattice coordinates.

In parton space, the linear actions of the space-group symmetries are straightforward since they simply modify the site indices. However, the action of  $\Theta$  has to be defined more carefully. Under time reversal, we have  $\Theta : \{f_{i\uparrow} \rightarrow -f_{i\downarrow}^\dagger, f_{i\downarrow} \rightarrow f_{i\uparrow}^\dagger\}$ , or equivalently, on the spinor doublet,  $\Theta : \psi_i \rightarrow \psi_i i\tau^y$ . Accordingly, the spin operators transform as

$$\begin{aligned} S_i^\gamma &= \frac{1}{2} \text{Tr} \left[ \psi_i^\dagger \tau^\gamma \psi_i \right] \rightarrow \frac{1}{2} \text{Tr} \left[ (-i\tau^y) \psi_i^\dagger (\tau^\gamma)^* \psi_i (i\tau^y) \right] \\ &= \frac{1}{2} \text{Tr} \left[ \psi_i^\dagger (\tau^\gamma)^* \psi_i \right] = (-1)^{\delta_{\gamma,y}} S_i^\gamma. \end{aligned}$$

The projective extension of the symmetry group can

be directly read off from Ref. 1 as:

$$W_{T_1}(x, y, s) = \eta^y \tau^0, \quad W_{T_2}(x, y, s) = \tau^0, \quad (\text{S6})$$

$$W_{C_6}(x, y, s) = \eta^{xy + \frac{y}{2}(y+1)} (\eta_{C_6})^{\delta_{s,6}} \tau^0, \quad (\text{S7})$$

$$W_R(x, y, s) = \eta^{\frac{x}{2}(x+1)} (\eta_{C_6})^{\delta_{s,5}} (\eta_{C_6R})^{\delta_{\text{mod}(s,2),0}} g_R, \quad (\text{S8})$$

$$W_\Theta(x, y, s) = \eta_{\Theta C_6}^s g_\Theta, \quad g_R^2 = \eta_R \tau^0, \quad (\text{S9})$$

where  $(x, y, s)$  denotes the position of a site on sublattice  $s$  in the unit cell located at  $(x, y)$ . In the equations above, all the parameters  $\{\eta, \eta_{C_6}, \eta_R, \eta_{C_6R}, \eta_{\Theta C_6}\}$  can take values  $\pm 1$  and the gauge-independent choices of the matrices  $g_R$  and  $g_\Theta$  are listed in Table I below. In total, we obtain 64 projective symmetry extensions for a  $\mathbb{Z}_2$  IGG.

$\eta_R$	$g_R$	$g_\Theta$	Set of $\eta$ parameters	# of PSGs
+1	$\tau^0$	$i\tau^y$	$\{\eta_{\Theta C_6}, \eta, \eta_{C_6}, \eta_{C_6R}\}$	$2^4$
+1	$\tau^0$	$\tau^0$	$\{\eta_{\Theta C_6} = -1, \eta, \eta_{C_6}, \eta_{C_6R}\}$	$2^3$
-1	$i\tau^z$	$i\tau^y$	$\{\eta_{\Theta C_6}, \eta, \eta_{C_6}, \eta_{C_6R}\}$	$2^4$
-1	$i\tau^z$	$i\tau^z$	$\{\eta_{\Theta C_6}, \eta, \eta_{C_6}, \eta_{C_6R}\}$	$2^4$
-1	$i\tau^z$	$\tau^0$	$\{\eta_{\Theta C_6} = -1, \eta, \eta_{C_6}, \eta_{C_6R}\}$	$2^3$

TABLE I. All possible gauge-inequivalent choices of the binary parameter  $\eta_R$ , and the two matrices  $g_R, g_\Theta$ , which together define a total of 64  $\mathbb{Z}_2$  PSG solutions.

Once the PSGs have been specified, we can proceed to construct the mean-field *Ansätze*. In our projective construction, the symmetries of the mean fields are preserved as

$$\begin{aligned} u_{ij}^0 &= (-1)^{\delta_{\mathcal{O},\Theta}} W_{\mathcal{O}}^\dagger(\mathcal{O}(i)) u_{\mathcal{O}(i)\mathcal{O}(j)}^0 W_{\mathcal{O}}(\mathcal{O}(j)), \\ u_{ij}^{\gamma'} &= W_{\mathcal{O}}^\dagger(\mathcal{O}(i)) u_{\mathcal{O}(i)\mathcal{O}(j)}^\gamma \mathcal{R}_{\mathcal{O}}^{\gamma'} W_{\mathcal{O}}(\mathcal{O}(j)), \end{aligned} \quad (\text{S10})$$

where  $\gamma, \gamma' = \{x, y, z\}$  and  $\mathcal{R}_{\mathcal{O}}$  are  $3 \times 3$  matrices. These matrices are, in general, nontrivial for real spin operators which transform as pseudovectors under symmetry operations. In our case, however, for the lattice space-group symmetry elements,  $\mathcal{R}_{\mathcal{O}} = \mathbb{1}_{3 \times 3}$ .

Now, let us consider the effect of time reversal on the *Ansatz*. For singlet fields, i.e.,  $u_{ij}^0 = is_{ij}^0 \tau^0 + s_{ij}^1 \tau^x +$



$s_{ij}^2 \tau^y + s_{ij}^3 \tau^z$ , we have

$$\begin{aligned} \Theta : \text{Tr} \left[ \psi_i u_{ij}^0 \psi_j^\dagger \right] &\rightarrow \text{Tr} \left[ \psi_i (i\tau^y) (u_{ij}^0)^* (-i\tau^y) \psi_j^\dagger \right] \\ &= - \text{Tr} \left[ \psi_i u_{ij}^0 \psi_j^\dagger \right], \end{aligned} \quad (\text{S11})$$

whereas for the triplet components, i.e.,  $u_{ij}^\gamma = t_{ij}^{\gamma,0} \tau^0 + i(t_{ij}^{\gamma,1} \tau^x + t_{ij}^{\gamma,2} \tau^y + t_{ij}^{\gamma,3} \tau^z)$ ,

$$\begin{aligned} \Theta : \text{Tr} \left[ \tau^\gamma \psi_i u_{ij}^\gamma \psi_j^\dagger \right] &\rightarrow \text{Tr} \left[ (\tau^\gamma)^* \psi_i (i\tau^y) (u_{ij}^\gamma)^* (-i\tau^y) \psi_j^\dagger \right] \\ &= (-)^{\delta_{\gamma,y}} \text{Tr} \left[ \tau^\gamma \psi_i u_{ij}^\gamma \psi_j^\dagger \right]. \end{aligned} \quad (\text{S12})$$

Therefore, we obtain

$$\Theta : u_{ij}^0 \rightarrow -u_{ij}^0, \quad (\text{S13})$$

$$\Theta : \{u_{ij}^x, u_{ij}^y, u_{ij}^z\} \rightarrow \{u_{ij}^x, -u_{ij}^y, u_{ij}^z\}, \quad (\text{S14})$$

so  $\mathcal{R}_\Theta = \text{Diag}[1, -1, 1]$  with an additional negative sign for the singlet fields.

As mentioned in the main text, the full spatial structure of the *Ansatz* can be defined by specifying a few

reference mean fields. Temporarily using the notation  $u_{s_1, s_2}^\alpha$  ( $s_1, s_2 = 1, \dots, 6$ ) to denote the directed link *from* a site on sublattice  $s_1$  *to* a site on sublattice  $s_2$ , the sign structure of the various terms is given by

$$u_{1,3}^\alpha = u_{2,4}^\alpha = \eta u_{3,5}^\alpha = \eta \eta_{C_6} u_{4,6}^\alpha = \eta \eta_{C_6} u_{5,1}^\alpha = \eta u_{6,2}^\alpha \equiv \mathcal{U}_1^\alpha, \quad (\text{S15})$$

$$u_{1,2}^\alpha = u_{2,3}^\alpha = u_{3,4}^\alpha = u_{4,5}^\alpha = \eta_{C_6} u_{5,6}^\alpha = u_{6,1}^\alpha \equiv \mathcal{U}_2^\alpha, \quad (\text{S16})$$

$$u_{1,4}^\alpha = \eta \eta_{C_6} u_{3,6}^\alpha = \eta \eta_{C_6} u_{5,2}^\alpha \equiv \mathcal{U}_3^\alpha, \quad (\text{S17})$$

$$u_{2,5}^\alpha = \eta \eta_{C_6} u_{4,1}^\alpha = \eta u_{6,3}^\alpha = \eta \eta_{C_6} \eta_{C_6 R} g_R^\dagger \mathcal{U}_3^\alpha g_R, \quad (\text{S18})$$

where the subscript 1, 2, or 3 on  $\mathcal{U}^\alpha$  indicates the first-, second-, or third-nearest-neighbor nature of the bond. Furthermore, the bonds connecting sites with different  $y$ -coordinates also change sign under translations by  $\mathbf{T}_1$ .

## III. MEAN-FIELD DECOUPLING

In the Abrikosov fermion representation  $S_i^\gamma = \frac{1}{2} f_{i\sigma}^\dagger \tau_{\sigma\sigma'}^\gamma f_{i\sigma'}$ , the Rydberg Hamiltonian can be recast as  $H = H_0 + H_2 + H_4$ , where

$$H_0 = -\frac{\Delta N}{2} + \sum_{\langle i,j \rangle} \frac{V_{ij}}{4}, \quad (\text{S19})$$

$$H_2 = \frac{1}{2} \sum_i \Omega f_{i,\sigma}^\dagger \tau_{\sigma\sigma'}^x f_{i,\sigma'} - \frac{1}{2} \sum_i \Delta f_{i,\sigma}^\dagger \tau_{\sigma\sigma'}^z f_{i,\sigma'} + \sum_{\langle i,j \rangle} \frac{V_{ij}}{4} \left[ f_{i,\sigma}^\dagger \tau_{\sigma\sigma'}^z f_{i,\sigma'} + f_{j,\sigma}^\dagger \tau_{\sigma\sigma'}^z f_{j,\sigma'} \right], \quad (\text{S20})$$

$$H_4 = \frac{1}{4} \sum_{\langle i,j \rangle} V_{ij} \sigma \sigma' f_{j\sigma'}^\dagger f_{i\sigma}^\dagger f_{i\sigma} f_{j\sigma'}. \quad (\text{S21})$$

Now, we perform a quadratic decoupling of the quartic term to obtain a mean-field theory as

$$\begin{aligned} \sigma \sigma' f_{j\sigma'}^\dagger f_{i\sigma}^\dagger f_{i\sigma} f_{j\sigma'} &= \langle f_{i\sigma}^\dagger f_{j\sigma}^\dagger \rangle f_{i\sigma} f_{j\sigma} + \langle f_{i\sigma} f_{j\sigma} \rangle f_{i\sigma}^\dagger f_{j\sigma}^\dagger - \langle f_{i\sigma}^\dagger f_{j\sigma}^\dagger \rangle \langle f_{i\sigma} f_{j\sigma} \rangle \\ &\quad - \langle f_{i\sigma}^\dagger f_{j\bar{\sigma}}^\dagger \rangle f_{i\sigma} f_{j\bar{\sigma}} - \langle f_{i\sigma} f_{j\bar{\sigma}} \rangle f_{i\sigma}^\dagger f_{j\bar{\sigma}}^\dagger + \langle f_{i\sigma}^\dagger f_{j\bar{\sigma}}^\dagger \rangle \langle f_{i\sigma} f_{j\bar{\sigma}} \rangle \\ &\quad - \langle f_{i\sigma}^\dagger f_{j\sigma} \rangle f_{j\sigma}^\dagger f_{i\sigma} - \langle f_{j\sigma}^\dagger f_{i\sigma} \rangle f_{i\sigma}^\dagger f_{j\sigma} + \langle f_{i\sigma}^\dagger f_{j\sigma} \rangle \langle f_{j\sigma}^\dagger f_{i\sigma} \rangle \\ &\quad + \langle f_{i\sigma}^\dagger f_{j\bar{\sigma}} \rangle f_{j\bar{\sigma}}^\dagger f_{i\sigma} + \langle f_{j\bar{\sigma}}^\dagger f_{i\sigma} \rangle f_{i\sigma}^\dagger f_{j\bar{\sigma}} - \langle f_{i\sigma}^\dagger f_{j\bar{\sigma}} \rangle \langle f_{j\bar{\sigma}}^\dagger f_{i\sigma} \rangle \\ &\quad + \langle \sigma f_{i\sigma}^\dagger f_{i\sigma} \rangle \sigma' f_{j\sigma'}^\dagger f_{j\sigma'} + \langle \sigma' f_{j\sigma'}^\dagger f_{j\sigma'} \rangle \sigma f_{i\sigma}^\dagger f_{i\sigma} - \langle \sigma f_{i\sigma}^\dagger f_{i\sigma} \rangle \langle \sigma' f_{j\sigma'}^\dagger f_{j\sigma'} \rangle. \end{aligned} \quad (\text{S22})$$

Next, we define the following singlet and triplet hopping and pairing fields:

$$\chi_{ij} = f_{i\uparrow}^\dagger f_{j\uparrow} + f_{i\downarrow}^\dagger f_{j\downarrow}, \quad \xi_{ij} = f_{i\uparrow}^\dagger f_{j\downarrow}^\dagger - f_{i\downarrow}^\dagger f_{j\uparrow}^\dagger, \quad (\text{S23})$$

$$T_{ij}^{x,h} = f_{i\uparrow}^\dagger f_{j\downarrow} + f_{i\downarrow}^\dagger f_{j\uparrow}, \quad T_{ij}^{y,h} = -i(f_{i\uparrow}^\dagger f_{j\downarrow} - f_{i\downarrow}^\dagger f_{j\uparrow}), \quad T_{ij}^{z,h} = f_{i\uparrow}^\dagger f_{j\uparrow} - f_{i\downarrow}^\dagger f_{j\downarrow}, \quad (\text{S24})$$

$$T_{ij}^{x,p} = f_{i\downarrow}^\dagger f_{j\downarrow}^\dagger - f_{i\uparrow}^\dagger f_{j\uparrow}^\dagger, \quad T_{ij}^{y,p} = i(f_{i\downarrow}^\dagger f_{j\downarrow}^\dagger + f_{i\uparrow}^\dagger f_{j\uparrow}^\dagger), \quad T_{ij}^{z,p} = f_{i\uparrow}^\dagger f_{j\downarrow}^\dagger + f_{i\downarrow}^\dagger f_{j\uparrow}^\dagger. \quad (\text{S25})$$

In the mean-field approximation, i.e.,  $\langle \chi_{ij} \rangle = \chi_{ij}$ ,  $\langle \xi_{ij} \rangle = \xi_{ij}$ , and  $\langle T_{ij}^{\gamma,r} \rangle = T_{ij}^{\gamma,r}$  (with  $r = h, p$ ), the Hamiltonian reads

$$H = H_0 + H_2 + H_2, \quad (\text{S26})$$

where

$$H_{\bar{0}} = H_0 + \frac{1}{8} \sum_{\langle i,j \rangle} V_{ij} \left[ |\chi_{ij}|^2 + |\xi_{ij}|^2 + \frac{1}{8} \sum_{\gamma,r} \zeta_\gamma |T_{ij}^{\gamma,r}|^2 - 2T_{ii}^{z,h} T_{jj}^{z,h} \right], \quad (\text{S27})$$

$$H_2 = \frac{1}{2} \sum_i \Omega T_{ii}^{x,h} - \frac{1}{2} \sum_i \Delta T_{ii}^{z,h} + \sum_{\langle i,j \rangle} \frac{V_{ij}}{4} [T_{ii}^{z,h} + T_{jj}^{z,h}], \quad (\text{S28})$$

$$H_{\bar{2}} = -\frac{1}{8} \sum_{\langle i,j \rangle} V_{ij} \left[ \left( \chi_{ij}^* \chi_{ij} + \xi_{ij}^* \xi_{ij} + \sum_{\gamma,r} \zeta_\gamma (T_{ij}^{\gamma,r})^* T_{ij}^{\gamma,r} + \text{h.c.} \right) - 2T_{ii}^{z,h} T_{jj}^{z,h} - 2T_{jj}^{z,h} T_{ii}^{z,h} \right], \quad (\text{S29})$$

with  $\zeta_z = -\zeta_x = -\zeta_y = +1$ . Now, using the doublet  $\psi_i$  and the matrices

$$u_{ij}^0 = \begin{bmatrix} \chi_{ij} & \xi_{ij} \\ \xi_{ij}^* & -\chi_{ij}^* \end{bmatrix}, \quad u_{ij}^\gamma = \begin{bmatrix} T_{ij}^{\gamma,h} & T_{ij}^{\gamma,p} \\ -(T_{ij}^{\gamma,p})^* & (T_{ij}^{\gamma,h})^* \end{bmatrix}, \quad (\text{S30})$$

one can rewrite the quadratic part, i.e.,  $H_q = H_2 + H_{\bar{2}}$ , in the form

$$H_q = \frac{1}{16} \sum_{\langle i,j \rangle} V_{ij} \left( \text{Tr}[\tau^\alpha \psi_i u_{ij}^\alpha \psi_j^\dagger + \text{h.c.}] + \text{Tr}[\tau^z \psi_i u_{ii}^z \psi_i^\dagger] + \text{Tr}[\tau^z \psi_j u_{jj}^z \psi_j^\dagger] \right) + \frac{1}{4} \sum_i \left( \Omega \text{Tr}[\tau^x \psi_i \psi_i^\dagger] - \Delta \text{Tr}[\tau^z \psi_i \psi_i^\dagger] \right), \quad (\text{S31})$$

where  $u_{ii}^z$  is a  $2 \times 2$  diagonal matrix with elements  $\tilde{T}_{ii}^{z,h}$  and  $(\tilde{T}_{ii}^{z,h})^\dagger$ ;  $\tilde{T}_{ii}^{z,h} \equiv 2T_{ii}^{z,h} + 1$ . If we also restrict the Hamiltonian to  $m^{\text{th}}$ -nearest-neighbor ( $m$ NN) terms and there are, say,  $N_p$   $p$ NN sites per unit cell, then we have

$$\begin{aligned} H_q &= \frac{1}{16} \sum_{p=1}^m \sum_{\langle i,j \rangle_p} V_p \left( \text{Tr}[\tau^\alpha \psi_i u_{ij}^\alpha \psi_j^\dagger + \text{h.c.}] + N_p \text{Tr}[\tau^z \psi_i u_{ii}^z \psi_i^\dagger] \right) + \frac{1}{4} \sum_i \left( \Omega \text{Tr}[\tau^x \psi_i \psi_i^\dagger] - \Delta \text{Tr}[\tau^z \psi_i \psi_i^\dagger] \right) \\ &= \frac{1}{16} \sum_{p=1}^m \sum_{\langle i,j \rangle_p} V_p \left( \text{Tr}[\tau^\alpha \psi_i u_{ij}^\alpha \psi_j^\dagger + \text{h.c.}] \right) + \frac{1}{4} \sum_i \left( \Omega \text{Tr}[\tau^x \psi_i \psi_i^\dagger] + \text{Tr}[\tau^z \psi_i \tilde{u}_{ii}^z \psi_i^\dagger] \right), \end{aligned} \quad (\text{S32})$$

where we use the shorthand  $\tilde{u}_{ii}^z \equiv -\Delta \tau^0 + u_{ii}^z \sum_{p=1}^m N_p V_p / 8$ , and  $V_p$  is the van der Waals interaction between  $p^{\text{th}}$ -neighboring sites. Note that each  $u_{ij}^\alpha$  consists of a hopping and a pairing field which are, in general, complex. Additionally, we denote  $u_{ii}^x = \Omega \tau^0$ , rename  $\tilde{u}_{ij}^z$  as  $u_{ij}^z$ , and absorb the constants by rescaling the  $u$  fields. This sequence of steps then finally brings us to expression for the quadratic Hamiltonian in Eq. (2) of the main text:

$$H_q = \sum_{p=1}^m \sum_{\langle i,j \rangle_p} V_p \text{Tr} \left[ \tau^\alpha \psi_i u_{ij}^\alpha \psi_j^\dagger + \text{h.c.} \right] + \sum_{i,\alpha=\{x,y,z\}} \text{Tr} \left[ \tau^\alpha \psi_i u_{ii}^\alpha \psi_i^\dagger \right]. \quad (\text{S33})$$

### SIII. SPIN STRUCTURE FACTORS

In this section, we first outline the procedure to calculate the spin structure factors in the fermionic spinon representation. Considering only the longitudinal component, the dynamical structure factor is defined as

$$\mathcal{S}(\mathbf{q}, \omega) = \int_{-\infty}^{+\infty} \frac{dt}{2\pi N^2} e^{i\omega t} \sum_{i,j} e^{i\mathbf{q} \cdot \mathbf{r}_{ij}} \left( \langle S_i^z(t) S_j^z(0) \rangle - \langle S_i^z(t) \rangle \langle S_j^z(0) \rangle \right) \equiv \mathcal{S}_{\text{tot}}(\mathbf{q}, \omega) - \mathcal{S}_{\text{dis}}(\mathbf{q}, \omega), \quad (\text{S34})$$

where  $\mathbf{r}_{ij} \equiv \mathbf{r}_i - \mathbf{r}_j$  and  $N$  is the total number of spins. In this definition, the connected correlator  $\mathcal{S}(\mathbf{q}, \omega)$  is interpreted as the sum of two pieces:  $\mathcal{S}_{\text{tot}}(\mathbf{q}, \omega)$ , which is the ‘‘total’’ correlation function  $\langle S_i^z(t) S_j^z(0) \rangle$ , and a disconnected part,  $\mathcal{S}_{\text{dis}}(\mathbf{q}, \omega)$ . Later, we will show how the disconnected contribution can be exactly canceled out by considering only the connected scattering mechanism.

To begin, substituting  $S_i^z(t) = e^{iHt} S_i^z e^{-iHt}$  in terms of the fermion operators,  $\mathcal{S}_{\text{tot}}(\mathbf{q}, \omega)$  is easily reformulated to

$$\mathcal{S}_{\text{tot}}(\mathbf{q}, \omega) = \int_{-\infty}^{+\infty} \frac{dt}{8\pi N^2} e^{i\omega t} \sum_{i,j} e^{i\mathbf{q}\cdot\mathbf{r}_{ij}} \tau_{\sigma\sigma}^z \tau_{\sigma'\sigma'}^z \sum_{\sigma,\sigma'} \left\langle e^{iHt} f_{i,\sigma}^\dagger f_{i,\sigma} e^{-iHt} f_{j,\sigma'}^\dagger f_{j,\sigma'} \right\rangle. \quad (\text{S35})$$

Before proceeding further, however, let us examine the generic structure of the quadratic spinon Hamiltonian. To do so, we consider the Bogoliubov–de Gennes(BdG) basis:

$$\psi = \left( \psi_\uparrow, \psi_\downarrow, (\psi_\uparrow^\dagger)^\text{T}, (\psi_\downarrow^\dagger)^\text{T} \right)^\text{T}; \quad \psi_\sigma = \left( f_{1,\sigma}, f_{2,\sigma}, \dots, f_{N,\sigma} \right). \quad (\text{S36})$$

Any general mean-field Hamiltonian can always be expressed in the form  $H = \psi^\dagger H_{\text{BdG}} \psi$ . The eigenvalues come in positive and negative pairs  $(\pm\epsilon_{\mu,\sigma})$  and, in the diagonal basis (obtained via a  $4N \times 4N$  unitary transformation  $U$ ),

$$\phi = \left( \phi_\uparrow, \phi_\downarrow, (\phi_\uparrow^\dagger)^\text{T}, (\phi_\downarrow^\dagger)^\text{T} \right)^\text{T}, \quad \psi_\sigma = \left( c_{1,\sigma}, c_{2,\sigma}, \dots, c_{N,\sigma} \right), \quad (\text{S37})$$

the BdG Hamiltonian takes the form

$$H_{\text{BdG}}^d = U^\dagger H_{\text{BdG}} U = \sum_{\mu=1}^N \sum_{\sigma=\uparrow,\downarrow} \epsilon_{\mu,\sigma} \left( c_{\mu,\sigma}^\dagger c_{\mu,\sigma} - c_{\mu,\sigma} c_{\mu,\sigma}^\dagger \right) = \sum_{\mu=1}^N \sum_{\sigma=\uparrow,\downarrow} \epsilon_{\mu,\sigma} \left( 2c_{\mu,\sigma}^\dagger c_{\mu,\sigma} - 1 \right). \quad (\text{S38})$$

This construction permits us to straightforwardly interpret the Bogoliubov quasiparticles as excitations with positive energy. Thus, the Fermi level lies at zero energy, and the ground state has no Bogoliubov excitations, by definition. The associated energy eigenvalues can also be listed as

$$\left( \dots, \epsilon_{m,\uparrow}, \dots, \epsilon_{m,\downarrow}, \dots, \epsilon_{m,\uparrow}, \dots, \epsilon_{m,\downarrow}, \dots \right) \equiv \left( \dots, \epsilon_m, \dots, \epsilon_{m+N}, \dots, \epsilon_{m+2N}, \dots, \epsilon_{m+3N}, \dots \right), \quad (\text{S39})$$

and this is the notation we use hereafter. In terms of the new  $c$ -fermions, the original  $f$ -fermion operators are given by

$$\begin{aligned} f_{i,\uparrow} &= \sum_{\mu=1}^N \left( U_{i,\mu} c_{\mu,\uparrow} + U_{i,\mu+N} c_{\mu,\downarrow} + U_{i,\mu+2N} c_{\mu,\uparrow}^\dagger + U_{i,\mu+3N} c_{\mu,\downarrow}^\dagger \right), \\ f_{i,\downarrow} &= \sum_{\mu=1}^N \left( U_{i+N,\mu} c_{\mu,\uparrow} + U_{i+N,\mu+N} c_{\mu,\downarrow} + U_{i+N,\mu+2N} c_{\mu,\uparrow}^\dagger + U_{i+N,\mu+3N} c_{\mu,\downarrow}^\dagger \right), \\ f_{i,\uparrow}^\dagger &= \sum_{\mu=1}^N \left( U_{i+2N,\mu} c_{\mu,\uparrow} + U_{i+2N,\mu+N} c_{\mu,\downarrow} + U_{i+2N,\mu+2N} c_{\mu,\uparrow}^\dagger + U_{i+2N,\mu+3N} c_{\mu,\downarrow}^\dagger \right), \\ f_{i,\downarrow}^\dagger &= \sum_{\mu=1}^N \left( U_{i+3N,\mu} c_{\mu,\uparrow} + U_{i+3N,\mu+N} c_{\mu,\downarrow} + U_{i+3N,\mu+2N} c_{\mu,\uparrow}^\dagger + U_{i+3N,\mu+3N} c_{\mu,\downarrow}^\dagger \right). \end{aligned} \quad (\text{S40})$$

This correspondence, as we now demonstrate, enables us to build up the spin structure factors piece-by-piece.

Consider first the term  $\mathcal{T}_{\sigma\sigma'} \equiv \left\langle e^{iHt} f_{i,\sigma}^\dagger f_{i,\sigma} e^{-iHt} f_{j,\sigma'}^\dagger f_{j,\sigma'} \right\rangle$  with  $\sigma = \sigma' = \uparrow$ . Using Eq. (S40), one can write

$$\begin{aligned} \mathcal{T}_{\uparrow\uparrow} &= \sum_{\mu,\nu,\rho,\lambda=1}^N \left\langle 0 \left| e^{iHt} \left( U_{i,\rho}^* c_{\rho,\uparrow}^\dagger + U_{i,\rho+N}^* c_{\rho,\downarrow}^\dagger + U_{i,\rho+2N}^* c_{\rho,\uparrow} + U_{i,\rho+3N}^* c_{\rho,\downarrow} \right) \right. \right. \\ &\quad \times \left( U_{i,\lambda} c_{\lambda,\uparrow} + U_{i,\lambda+N} c_{\lambda,\downarrow} + U_{i,\lambda+2N} c_{\lambda,\uparrow}^\dagger + U_{i,\lambda+3N} c_{\lambda,\downarrow}^\dagger \right) e^{-iHt} \\ &\quad \times \left( U_{j,\mu}^* c_{\mu,\uparrow}^\dagger + U_{j,\mu+N}^* c_{\mu,\downarrow}^\dagger + U_{j,\mu+2N}^* c_{\mu,\uparrow} + U_{j,\mu+3N}^* c_{\mu,\downarrow} \right) \\ &\quad \left. \times \left( U_{j,\nu} c_{\nu,\uparrow} + U_{j,\nu+N} c_{\nu,\downarrow} + U_{j,\nu+2N} c_{\nu,\uparrow}^\dagger + U_{j,\nu+3N} c_{\nu,\downarrow}^\dagger \right) \right| 0 \rangle. \end{aligned} \quad (\text{S41})$$

Recalling that the ground state is the Bogoliubov vacuum  $|0\rangle$ , a scattering process follows the creation of a pair of Bogoliubov quasiparticles at time 0 and their annihilation at a later time  $t$ . Therefore, the terms of the form

“ $c_{\rho,\sigma_1}(t)c_{\lambda,\sigma_2}(t)c_{\mu,\sigma'_1}^\dagger(0)c_{\nu,\sigma'_2}^\dagger(0)$ ” will contribute to the structure factors. On the other hand, this ensures the exclusion of the disconnected contributions, i.e.,  $\mathcal{S}_{\text{dis}}(\mathbf{q}, \omega)$  in Eq. (S34), arising from terms like “ $c_{\rho,\sigma_1}(t)c_{\rho,\sigma_1}^\dagger(t)c_{\mu,\sigma'_1}(0)c_{\mu,\sigma'_1}^\dagger(0)$ ” where the process follows the creation of quasiparticles  $(\mu, \sigma'_1)$  and  $(\rho, \sigma_1)$  at times 0 and  $t$ , respectively, followed by their annihilation at the same time.

The connected pieces, which we concentrate on, can be further simplified. To illustrate this, let us take, for example, the term  $\langle 0|e^{iHt}c_{\rho,\uparrow}c_{\lambda,\uparrow}e^{-iHt}c_{\mu,\uparrow}^\dagger c_{\nu,\uparrow}^\dagger|0\rangle$ , which contributes to the DSF as

$$\begin{aligned}
& \int_{-\infty}^{+\infty} \frac{dt}{8\pi N^2} e^{i\omega t} \sum_{i,j} e^{i\mathbf{q}\cdot\mathbf{r}_{ij}} \sum_{\mu,\nu,\rho,\lambda} U_{i,\rho+2N}^* U_{i,\lambda} U_{j,\mu}^* U_{j,\nu+2N} \langle 0|e^{iHt}c_{\rho,\uparrow}c_{\lambda,\uparrow}e^{-iHt}c_{\mu,\uparrow}^\dagger c_{\nu,\uparrow}^\dagger|0\rangle \\
&= \int_{-\infty}^{+\infty} \frac{dt}{8\pi N^2} e^{i\omega t} \sum_{i,j} e^{i\mathbf{q}\cdot\mathbf{r}_{ij}} \sum_{\mu,\nu,\rho,\lambda} U_{i,\rho+2N}^* U_{i,\lambda} U_{j,\mu}^* U_{j,\nu+2N} \langle 0|c_{\rho,\uparrow}c_{\lambda,\uparrow}c_{\mu,\uparrow}^\dagger c_{\nu,\uparrow}^\dagger|0\rangle e^{-i(\epsilon_\mu + \epsilon_{\nu+2N})t} \\
&= \frac{1}{4N^2} \sum_{i,j} e^{i\mathbf{q}\cdot\mathbf{r}_{ij}} \sum_{\mu,\nu,\rho,\lambda} U_{i,\rho+2N}^* U_{i,\lambda} U_{j,\mu}^* U_{j,\nu+2N} \langle 0|c_{\rho,\uparrow}c_{\lambda,\uparrow}c_{\mu,\uparrow}^\dagger c_{\nu,\uparrow}^\dagger|0\rangle \delta(\epsilon_\mu + \epsilon_{\nu+2N} - \omega) \\
&= \frac{1}{4N^2} \sum_{i,j} e^{i\mathbf{q}\cdot\mathbf{r}_{ij}} \sum_{\mu,\nu,\rho,\lambda} U_{i,\rho+2N}^* U_{i,\lambda} U_{j,\mu}^* U_{j,\nu+2N} (\delta_{\rho,\nu}\delta_{\lambda,\mu} - \delta_{\rho,\mu}\delta_{\lambda,\nu}) \delta(\epsilon_\mu + \epsilon_{\nu+2N} - \omega) \\
&= \frac{1}{4N^2} \sum_{i,j,\mu,\nu} e^{i\mathbf{q}\cdot\mathbf{r}_{ij}} (U_{i,\nu+2N}^* U_{i,\mu} - U_{i,\mu+2N}^* U_{i,\nu}) U_{j,\mu}^* U_{j,\nu+2N} \delta(\epsilon_\mu + \epsilon_{\nu+2N} - \omega). \tag{S42}
\end{aligned}$$

One can analogously derive all the other terms constituting  $\mathcal{T}_{\uparrow\uparrow}$ . Combining these, the net contribution of  $\mathcal{T}_{\uparrow\uparrow}$  to  $\mathcal{S}(\mathbf{q}, \omega)$  takes the following form:

$$\begin{aligned}
(\mathcal{S}(\mathbf{q}, \omega))_{\uparrow\uparrow} &= \frac{1}{4N^2} \sum_{i,j} e^{i\mathbf{q}\cdot\mathbf{r}_{ij}} \sum_{\mu,\nu} [(U_{i,\nu+2N}^* U_{i,\mu} - U_{i,\mu+2N}^* U_{i,\nu}) U_{j,\mu}^* U_{j,\nu+2N} \delta(\epsilon_\mu + \epsilon_{\nu+2N} - \omega) \\
&\quad + (U_{i,\nu+3N}^* U_{i,\mu+N} - U_{i,\mu+3N}^* U_{i,\nu+N}) U_{j,\mu+N}^* U_{j,\nu+3N} \delta(\epsilon_{\mu+N} + \epsilon_{\nu+3N} - \omega) \\
&\quad + (U_{i,\nu+2N}^* U_{i,\mu+N} - U_{i,\mu+3N}^* U_{i,\nu}) U_{j,\mu+N}^* U_{j,\nu+2N} \delta(\epsilon_{\mu+N} + \epsilon_{\nu+2N} - \omega) \\
&\quad + (U_{i,\nu+3N}^* U_{i,\mu} - U_{i,\mu+2N}^* U_{i,\nu+N}) U_{j,\mu}^* U_{j,\nu+3N} \delta(\epsilon_\mu + \epsilon_{\nu+3N} - \omega)] \\
&\equiv \frac{1}{4N^2} \sum_{i,j} e^{i\mathbf{q}\cdot\mathbf{r}_{ij}} g(i, j). \tag{S43}
\end{aligned}$$

Carrying out a similar analysis for the other components, i.e.,  $(\mathcal{S}(\mathbf{q}, \omega))_{\downarrow\downarrow}$ ,  $(\mathcal{S}(\mathbf{q}, \omega))_{\uparrow\downarrow}$ , and  $(\mathcal{S}(\mathbf{q}, \omega))_{\downarrow\uparrow}$ , one finds the full expression for the DSF to be

$$\mathcal{S}(\mathbf{q}, \omega) = \frac{1}{4N^2} \sum_{i,j} e^{i\mathbf{q}\cdot\mathbf{r}_{ij}} [g(i, j) + g(i + N, j + N) - g(i, j + N) - g(i + N, j)]. \tag{S44}$$

The static structure factor, which is the equal-time momentum-resolved spin-spin correlation function, can then directly be calculated from this equation as  $S(\mathbf{q}) = \sum_\omega \mathcal{S}(\mathbf{q}, \omega)$ .

Following the procedure outlined above, we systematically compute the static and dynamical structure factors for all our  $\mathbb{Z}_2$  QSL *Ansätze*, over a broad range of parameters, and these are presented in Figs. S1 through S6, and Figs. S7 to S12, respectively.

---

[1] A. Maity, R. Samajdar, and Y. Iqbal, Gapped and gapless quantum spin liquids on the ruby lattice (2024).

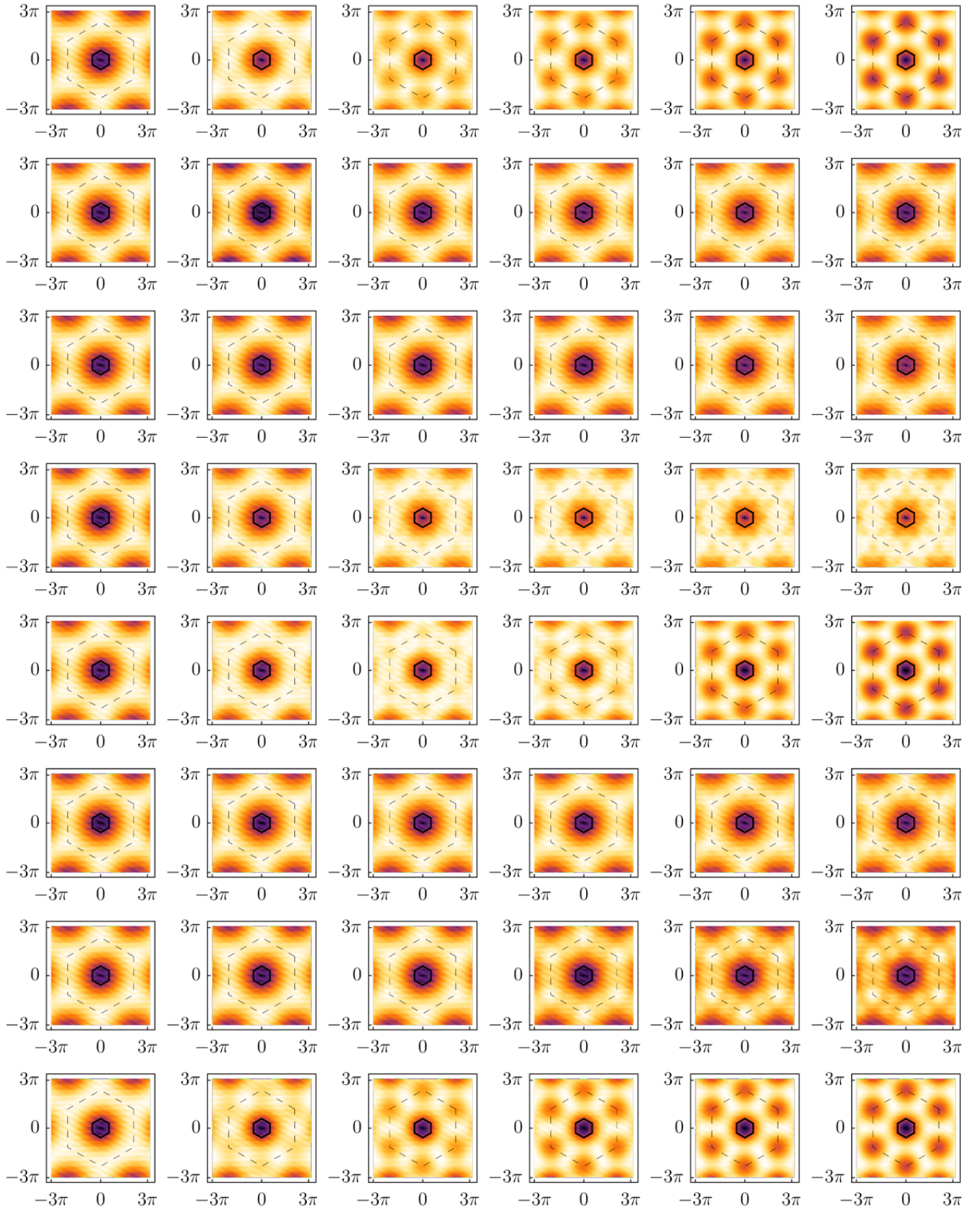


FIG. S1. Static structure factors for the  $\mathbb{Z}_2$  *Ansätze* listed in the first eight rows of Table I, with  $\eta_{C_6} = \eta = +1$ , for a system size of  $10 \times 10 \times 6$  sites. The mean-field parameters for the first-nearest-neighbor (1NN) and second-nearest-neighbor (2NN) bonds are chosen in the ratio  $1 : r$ , while those on the third-nearest-neighbor (3NN) bonds are set to zero. The six columns, from left to right, correspond to  $r = 0.25, 0.50, 0.75, 1.00, 1.25,$  and  $1.50$ , respectively. Without loss of generality, we choose an onsite triplet term of magnitude 0.2. The solid (dashed) hexagon marks the first (extended) Brillouin zone.

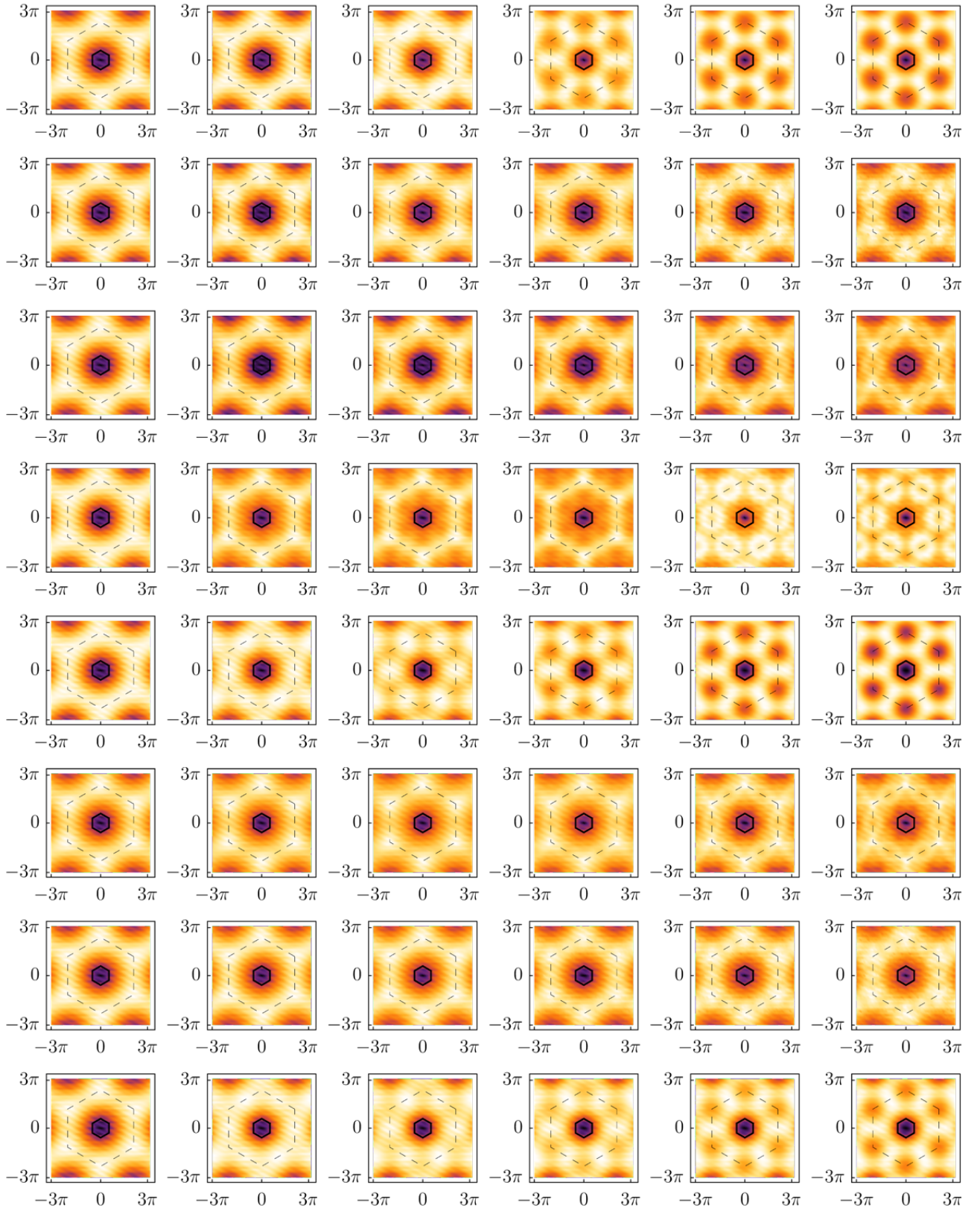


FIG. S2. Same as in Fig. S1 but for the  $Z_2$  Ansatz in the  $\eta_{C_6} = \eta = -1$  class.

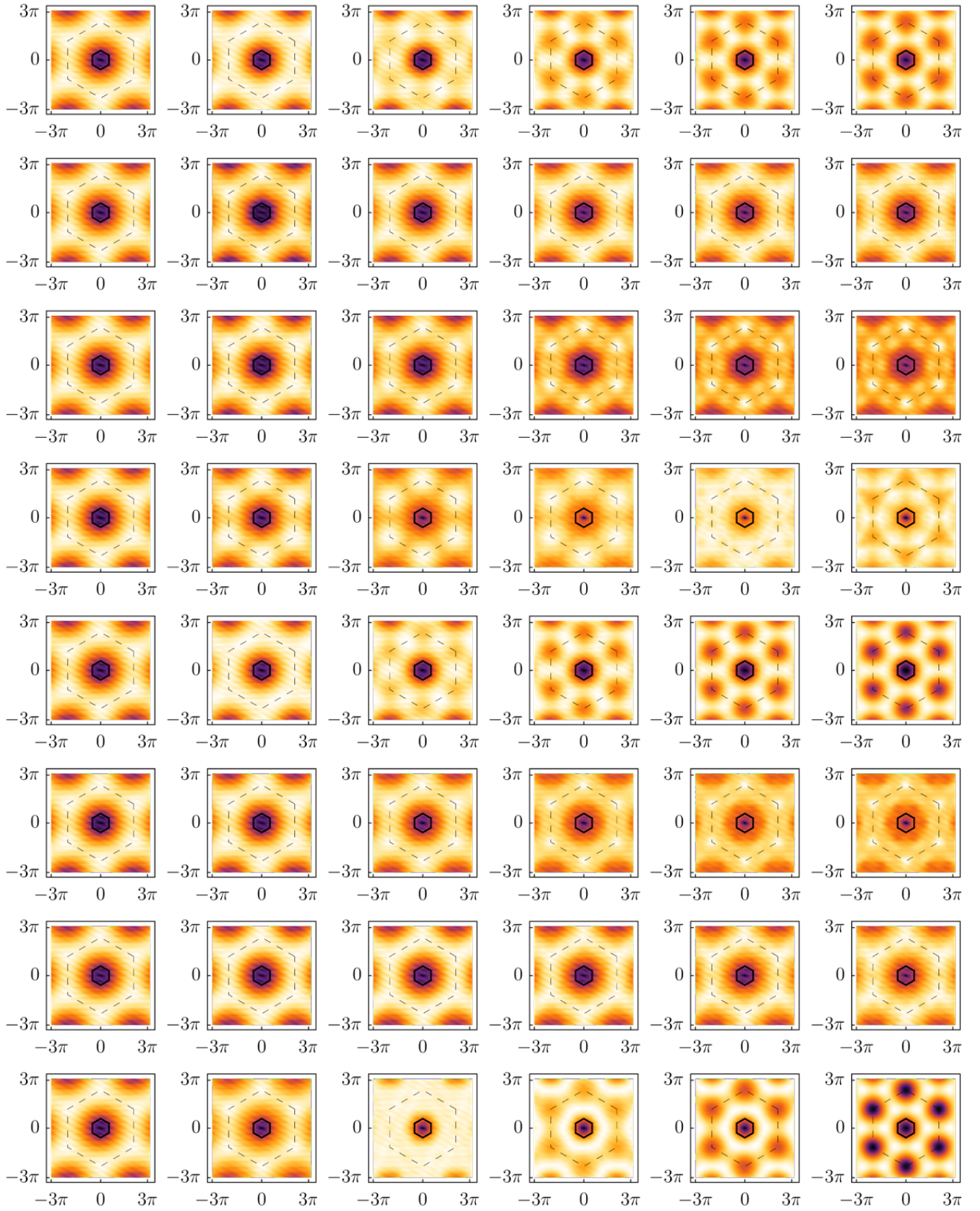


FIG. S3. Same as in Fig. S1 but for the  $\mathbb{Z}_2$  Ansätze in the  $\eta_{C_6} = -\eta = -1$  class.

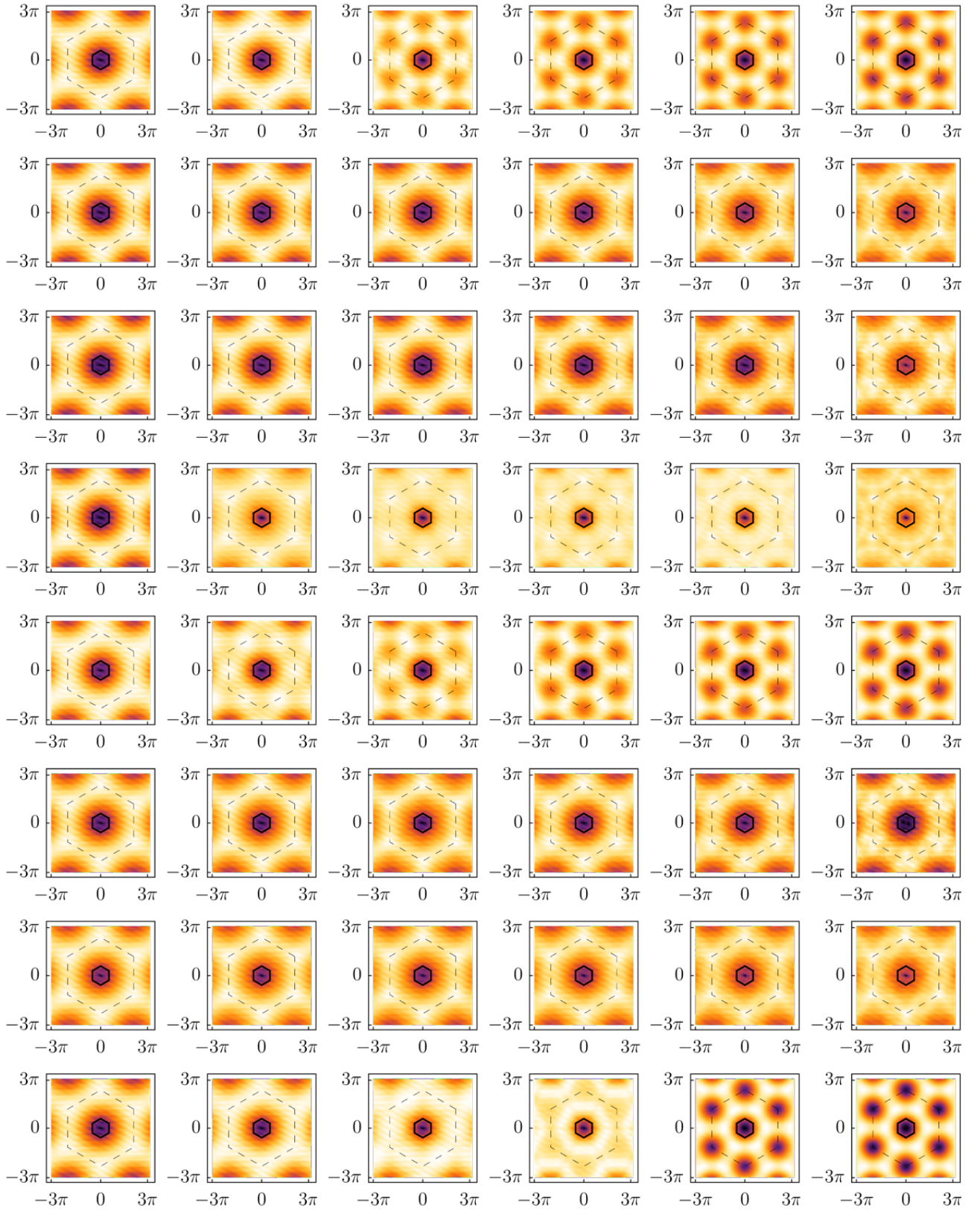


FIG. S4. Same as in Fig. S1 but for the  $\mathbb{Z}_2$  Ansätze in the  $\eta_{C_6} = -\eta = +1$  class.



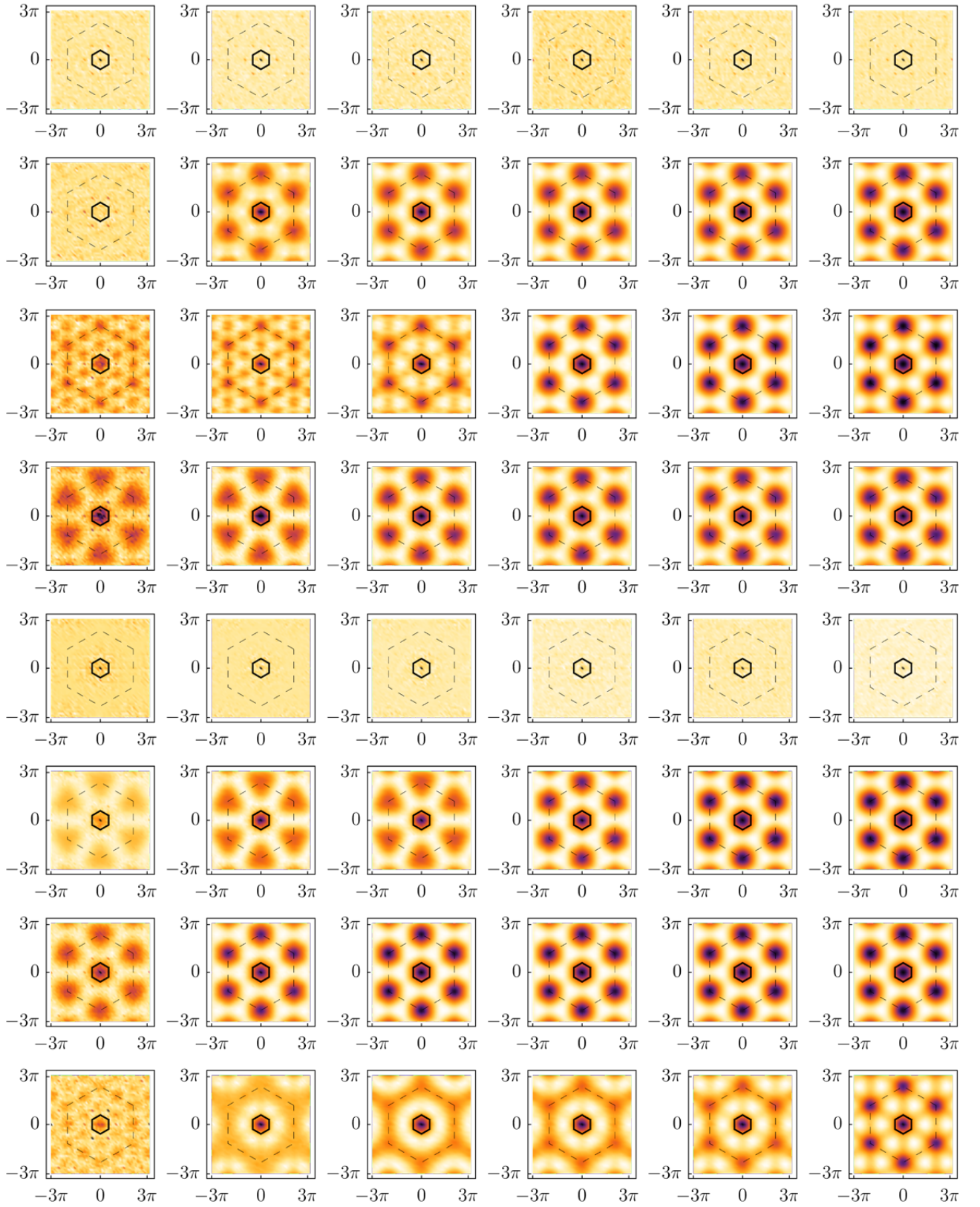


FIG. S5. Static structure factors for the  $\mathbb{Z}_2$  Ansatz listed in rows 9–12 of Table I, with  $\eta_{C_6} = \eta = +1$  (first four rows of the figure) and  $\eta_{C_6} = -\eta = -1$  (last four rows here). All other parameters and conventions are chosen to be the same as in Fig. S1.

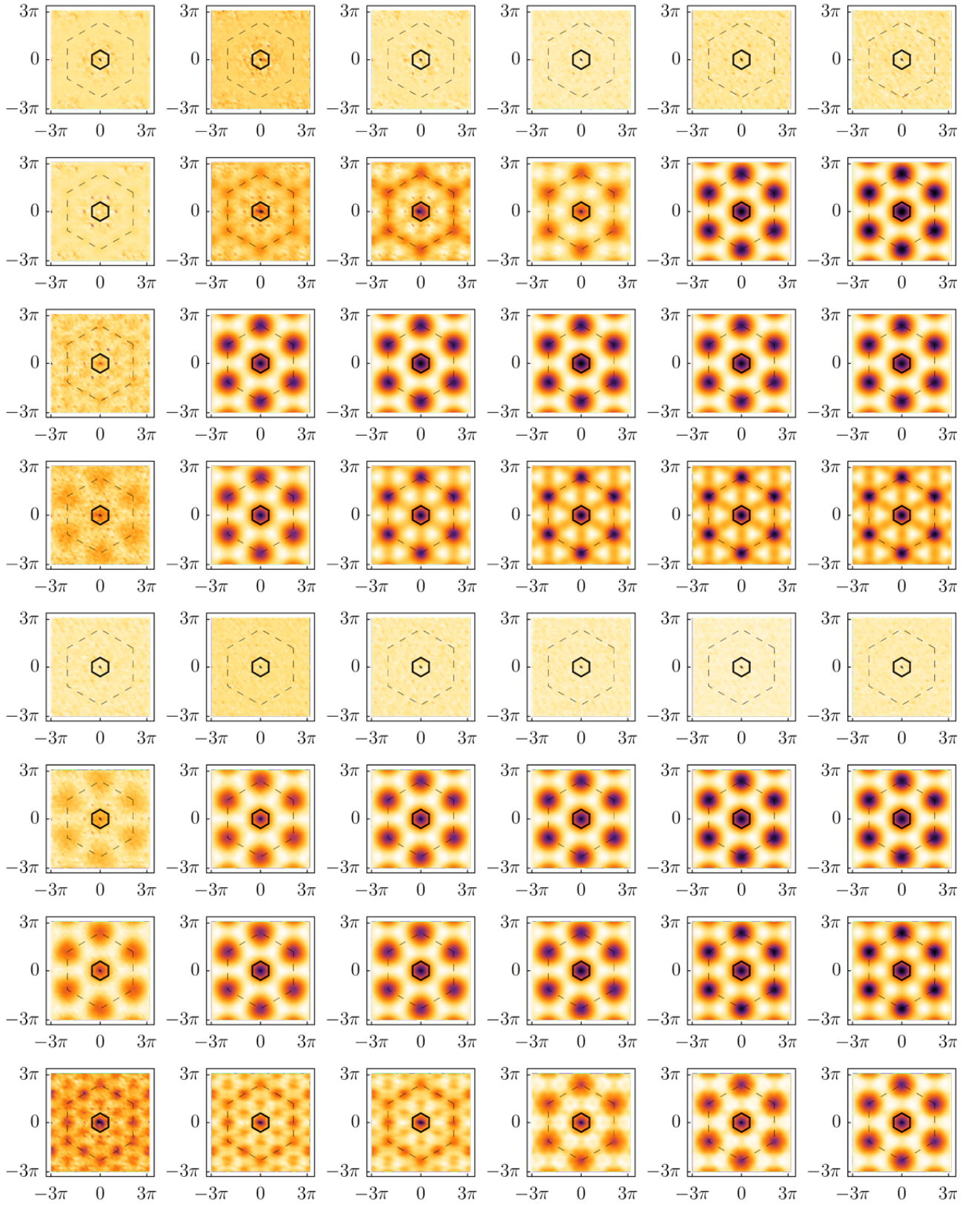


FIG. S6. Same as in Fig. S5, but for the  $\eta_{C_6} = \eta = -1$  (first four rows) and  $\eta_{C_6} = -\eta = +1$  (last four rows) classes.

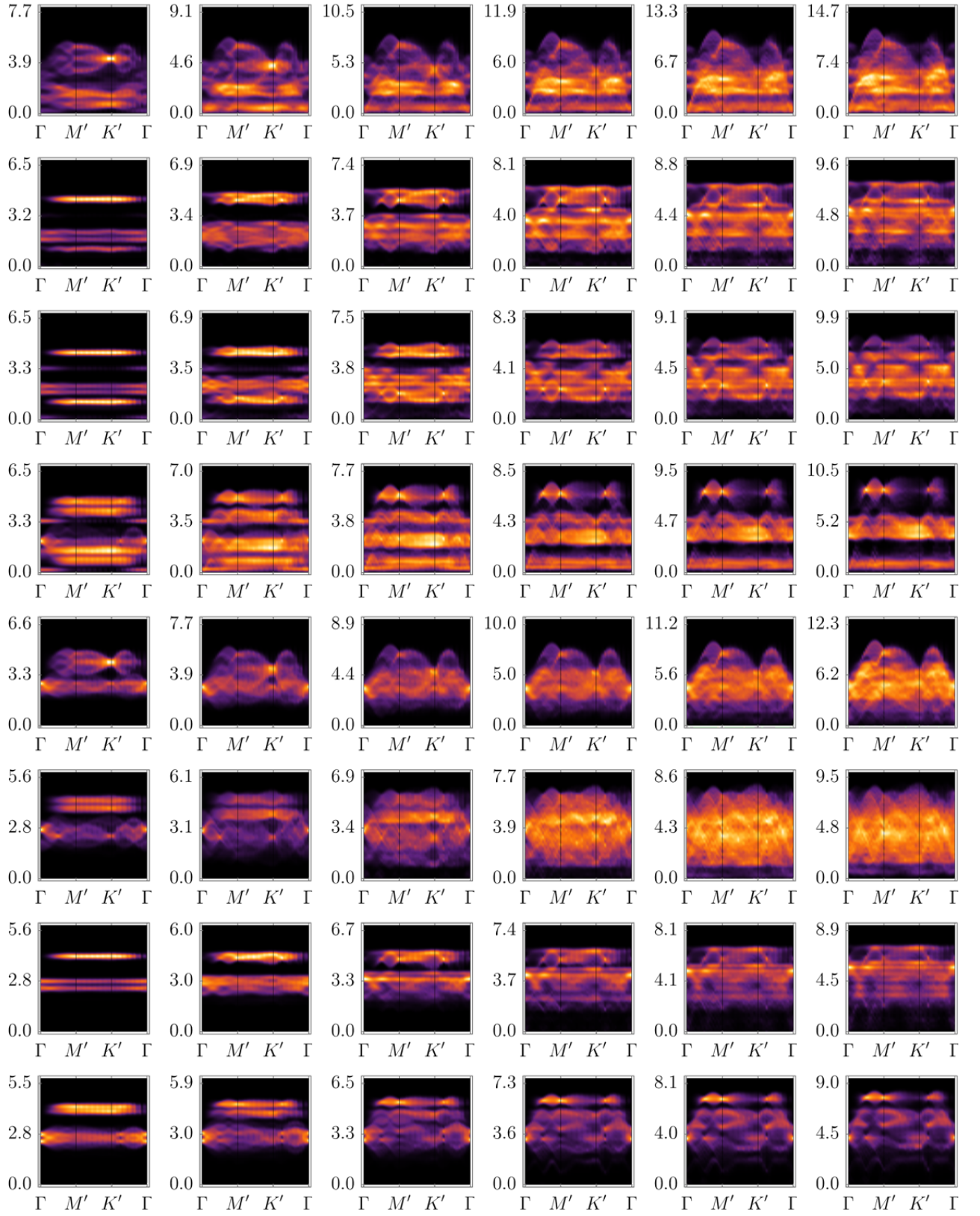


FIG. S7. Dynamical structure factors, plotted along a high-symmetry path in the extended Brillouin zone, for the  $\mathbb{Z}_2$  Ansatzes listed in the first eight rows of Table I, with  $\eta_{C_6} = \eta = +1$ . All parameters and conventions are chosen to be the same as in Fig. S1.

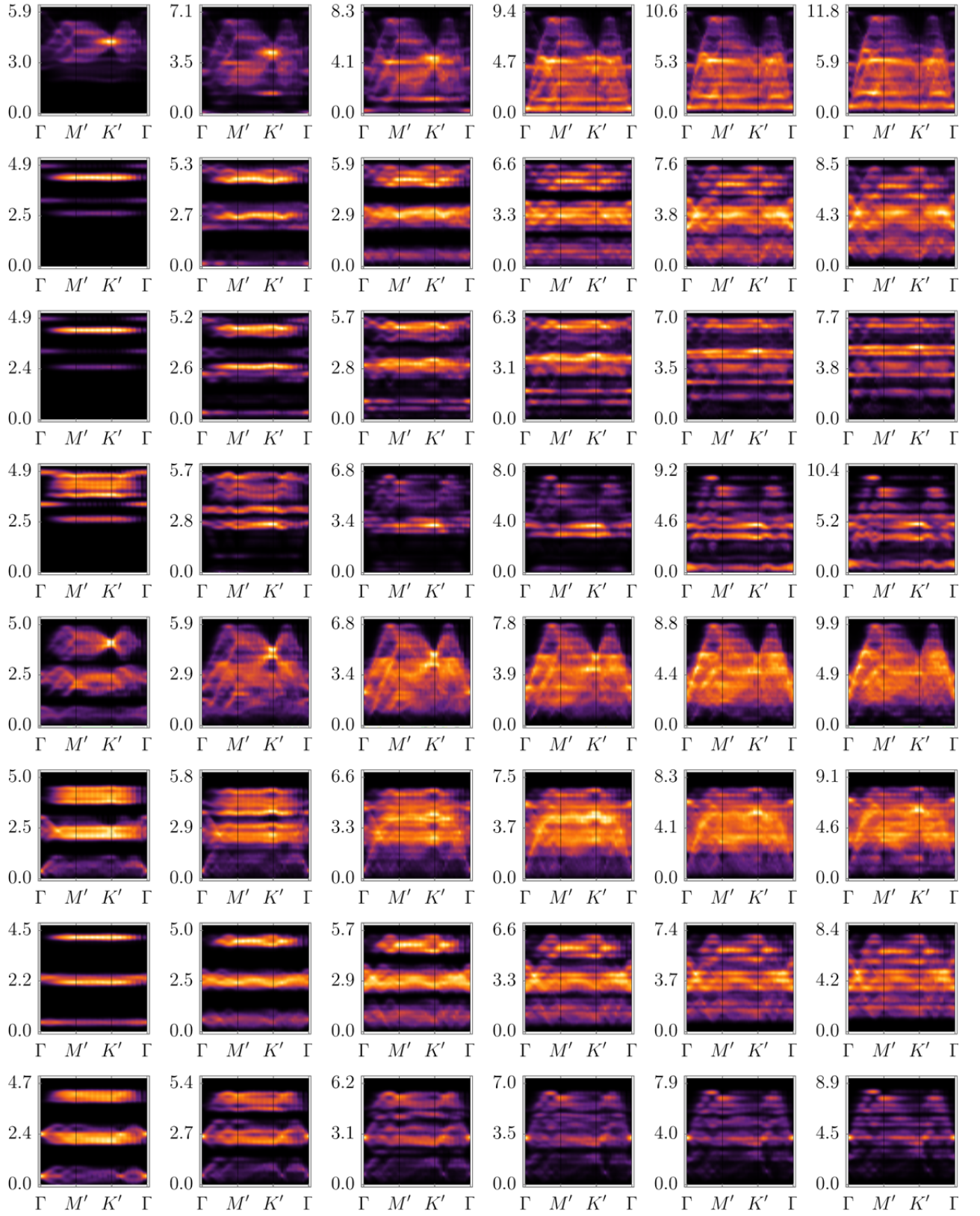


FIG. S8. Same as in Fig. S7 but for the  $\mathbb{Z}_2$  Ansätze in the  $\eta_{C_6} = \eta = -1$  class.

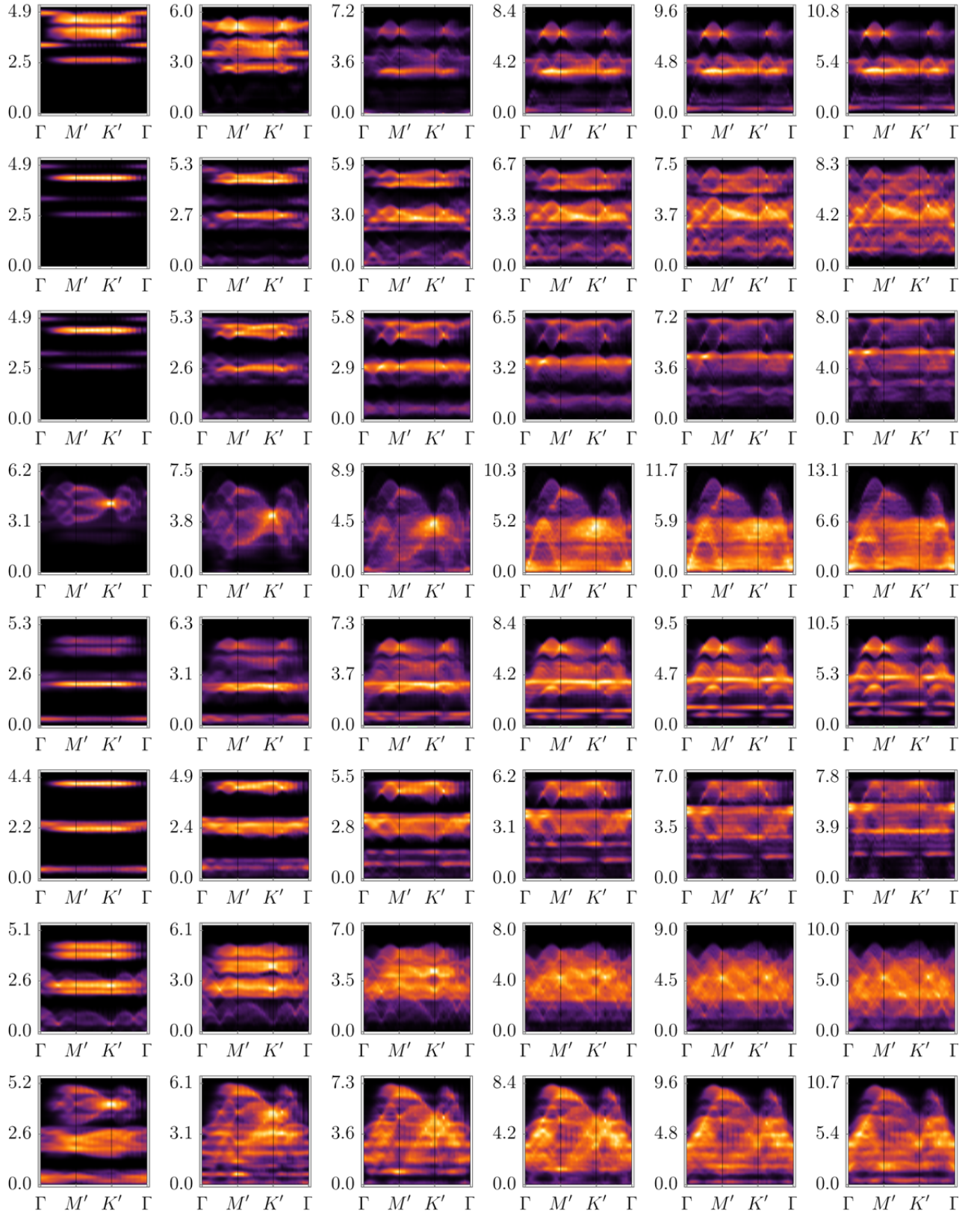


FIG. S9. Same as in Fig. S7 but for the  $\mathbb{Z}_2$  Ansatz in the  $\eta_{C_6} = -\eta = -1$  class.

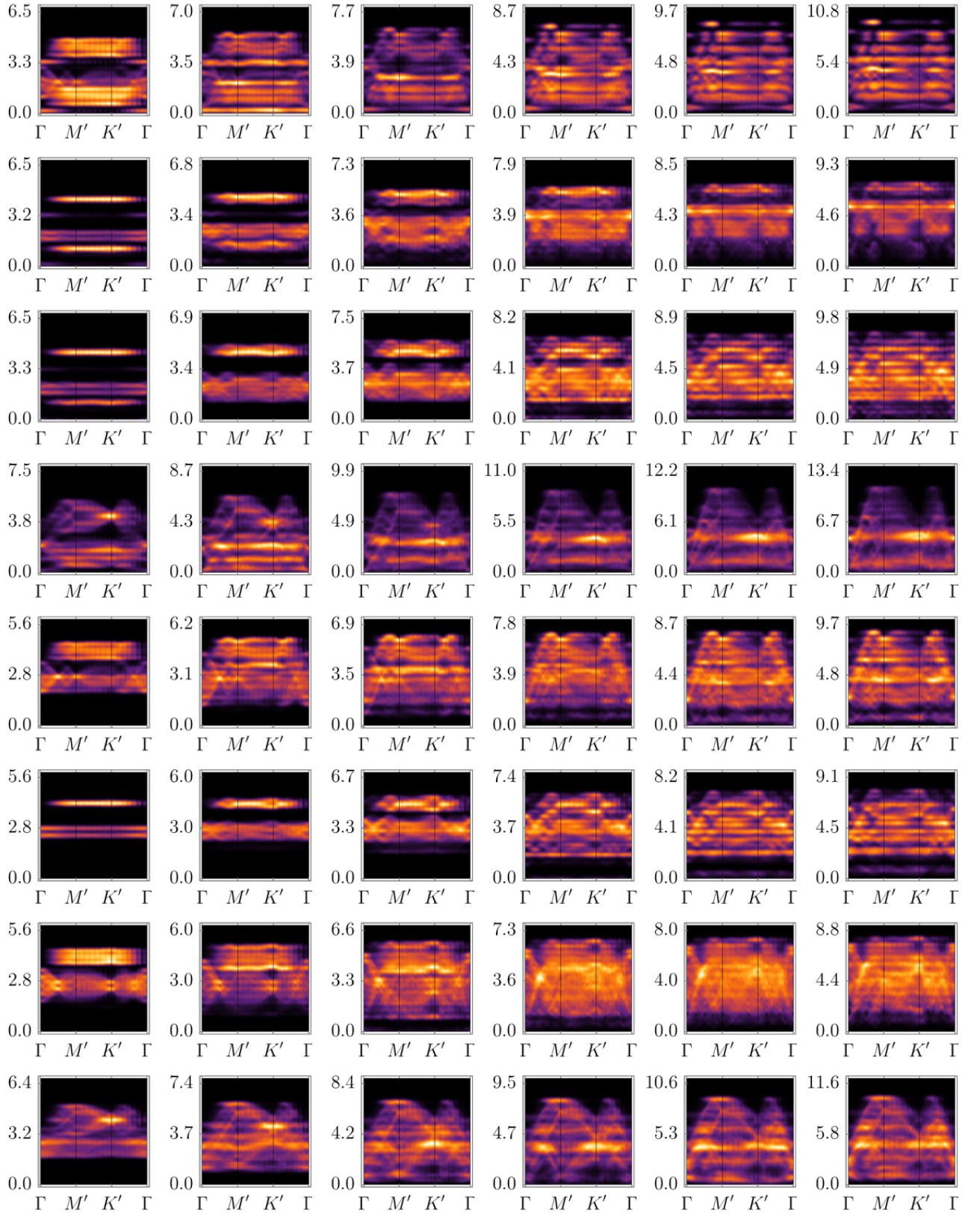


FIG. S10. Same as in Fig. S7 but for the  $\mathbb{Z}_2$  Ansätze in the  $\eta_{C_6} = -\eta = 1$  class.

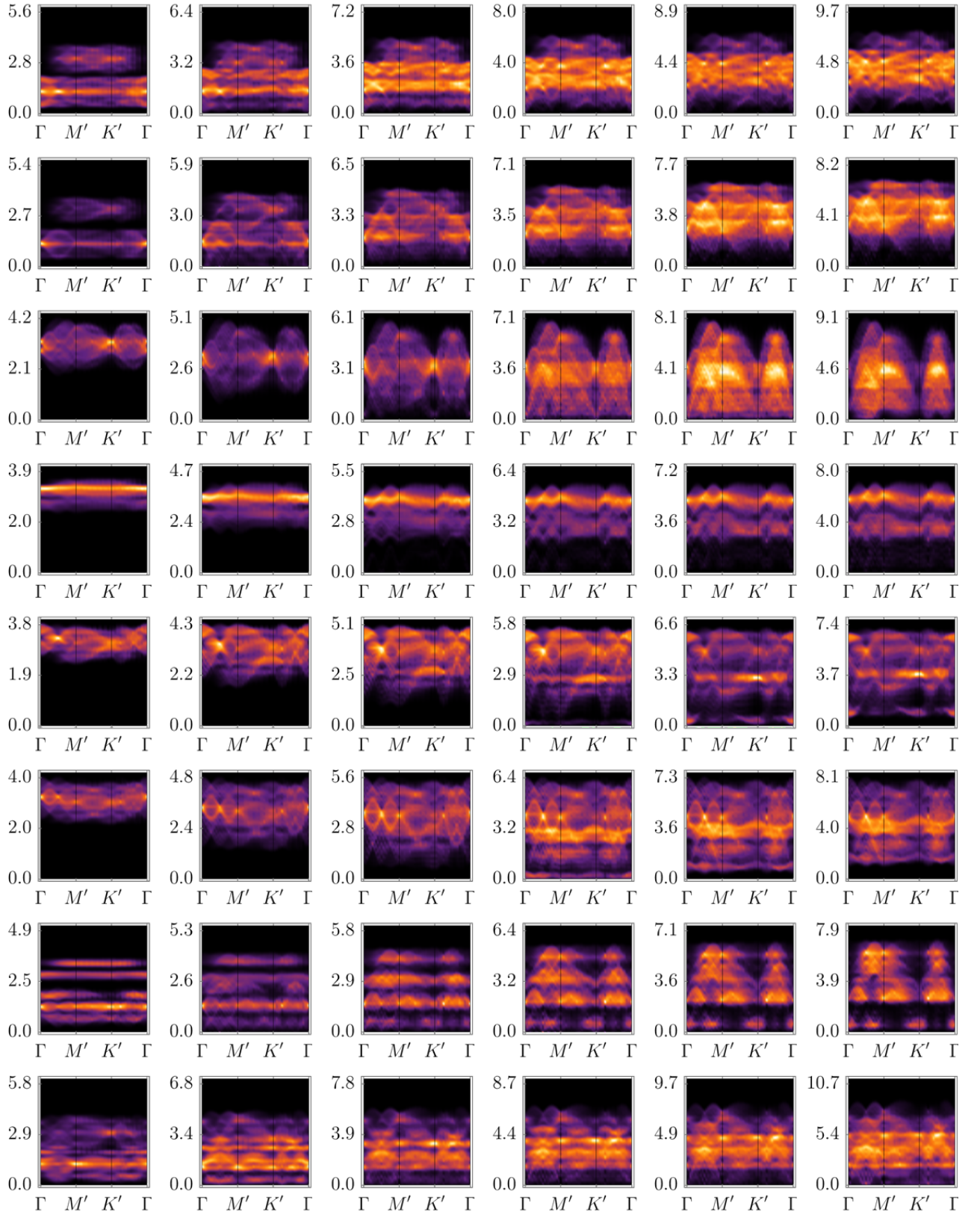


FIG. S11. Dynamical structure factors for the  $\mathbb{Z}_2$  *Ansätze* listed in rows 9–12 of Table I, with  $\eta_{C_6} = \eta = +1$  (first four rows of the figure) and  $\eta_{C_6} = -\eta = -1$  (last four rows here). All other parameters and conventions are taken to be the same as in Fig. S7.

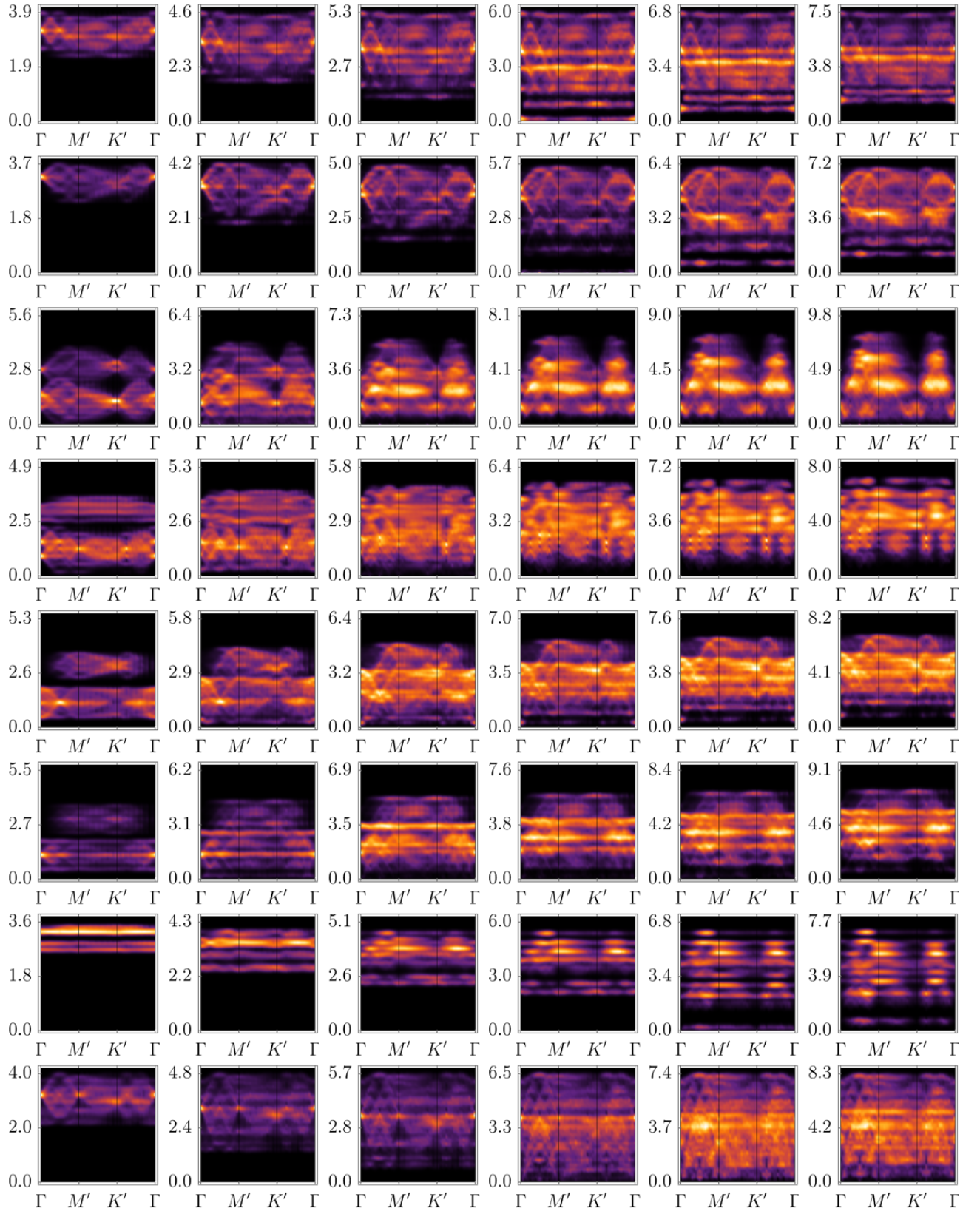


FIG. S12. Same as in Fig. S11 but for the  $\eta_{C_6} = \eta = -1$  (first four rows) and  $\eta_{C_6} = -\eta = +1$  (last four rows) classes.